Experimental ^{64}Zn($\vec{d}, t$)^{63}Zn spectroscopic factors: Guidance for isospin-symmetry-breaking calculations

K. G. Leach,[1,*] P. E. Garrett,[1,2] I. S. Towner,[3] G. C. Ball,[4] V. Bildstein,[1] B. A. Brown,[5,6] G. A. Demand,[1] T. Faestermann,[7] P. Finlay,[1,†] K. L. Green,[1] R. Hertenberger,[8] R. Krücken,[4,7] A. A. Phillips,[1] E. T. Rand,[1] C. S. Sumithrarachchi,[1,‡] C. E. Svensson,[1] S. Triambak,[1,§] H.-F. Wirth,[8] and J. Wong[1]

[1]*Department of Physics, University of Guelph, Guelph, Ontario N1G 2W1, Canada*
[2]*Excellence Cluster Universe, Boltzmannstrasse 2, D-85748 Garching, Germany*
[3]*Cyclotron Institute, Texas A&M University, College Station, Texas 77843-3366, USA*
[4]*TRIUMF, 4004 Wesbrook Mall, Vancouver, British Columbia V6T 2A3, Canada*
[5]*National Superconducting Cyclotron Laboratory, Michigan State University, East Lansing, Michigan 48824, USA*
[6]*Department of Physics and Astronomy, Michigan State University, East Lansing, Michigan 48824, USA*
[7]*Physik Department, Technische Universität München, D-85748 Garching, Germany*
[8]*Fakultät für Physik, Ludwig-Maximilians-Universität München, D-85748 Garching, Germany*

With the recent inclusion of core orbitals to the radial-overlap component of the isospin-symmetry-breaking (ISB) corrections for superallowed Fermi β decay, experimental data are needed to test the validity of the theoretical model. This work reports measurements of single-neutron pickup reaction spectroscopic factors into ^{63}Zn, one neutron away from ^{62}Zn, the superallowed daughter of ^{62}Ga. The experiment was performed using a 22-MeV polarized deuteron beam, a Q3D magnetic spectrograph, and a cathode-strip focal-plane detector to analyze outgoing tritons at nine angles between $10°$ and $60°$. Angular distributions and vector analyzing powers were obtained for all 162 observed states in ^{63}Zn, including 125 newly observed levels, up to an excitation energy of 4.8 MeV. Spectroscopic factors are extracted and compared to several shell-model predictions, and implications for the ISB calculations are discussed.

PACS number(s): 21.10.Jx, 21.60.Cs, 25.45.Hi, 27.50.+e

I. INTRODUCTION

There is an intense ongoing focus on experimental and theoretical studies of superallowed $0^+ \to 0^+$ nuclear β decays [1,2]. These currently provide the most precise determination of the vector coupling constant for weak interactions, G_V, which is vital in the extraction of the up-down element of the Cabibbo-Kobayashi-Maskawa (CKM) quark-mixing matrix, V_{ud}. In order to extract V_{ud} from the high-precision experimental data, corrections to the almost nucleus-independent ft values for superallowed β decays must be made for radiative effects as well as isospin symmetry breaking (ISB) by Coulomb and charge-dependent nuclear forces [3]. Although these corrections are small ($\sim$1%), experimental measurements have provided such precise ft values [1] ($\pm$0.03%) that the uncertainty on G_V is currently dominated by the precision of the theoretical corrections.

The transition-independent $\mathcal{F}t$ value is defined as [3]

$$\mathcal{F}t \equiv ft(1 + \delta_R)(1 - \delta_C) = \frac{K}{2G_V^2(1 + \Delta_R)}, \qquad (1)$$

where δ_R is a transition-dependent radiative correction, Δ_R is a transition-independent radiative correction, and δ_C is a nucleus-dependent ISB correction. The relative magnitudes for each of the correction terms, for the 13 $T = 1$ superallowed cases used in Ref. [1] to evaluate $\overline{\mathcal{F}t}$, are displayed in Fig. 1. Over the past ten years, significant experimental progress has been made in improving the accuracy and precision of the individual ft values used in this evaluation, which has led to the limiting uncertainty on the Standard-Model testing for most cases coming from the calculated δ_C values, as described in detail in Ref. [1].

The drastic improvement in experimental precision prompted a reevaluation of the calculation method of δ_C by Towner and Hardy in 2008 [3], in an attempt to decrease the theoretical uncertainties associated with the ISB correction, as well as improve the overall accuracy of each case. During this reevaluation, it was determined that a crucial aspect of the ISB calculation for ^{46}V was missing after carefully examining experimental spectroscopic factors from the ^{46}Ti(^{3}He, α)^{45}Ti reaction [4]. The authors of Ref. [3] found that by not including interactions within the core orbitals, they had missed a significant amount of single-neutron spectroscopic strengths, which, when included in the calculation model space, resulted in a δ_{C2} value that was nearly a factor of two larger than the previously accepted δ_{C2} value for ^{46}V in Ref. [5]. As a result, the δ_{C2} values reported in Ref. [3] use experimental single-neutron-pickup spectroscopic factors to guide the model-space truncations, specifically for heavier nuclei, where the model-space truncations become quite severe.

*Present address: TRIUMF, 4004 Wesbrook Mall, Vancouver, British Columbia V6T 2A3, Canada; kleach@triumf.ca

†Present address: Instituut voor Kern- en Stralingsfysica, K.U. Leuven, Celestijnenlaan 200D, B-3001 Leuven, Belgium.

‡Present address: National Superconducting Cyclotron Laboratory, Michigan State University, East Lansing, Michigan 48824, USA.

§Present address: Department of Physics, and Astrophysics, University of Delhi, Delhi 110 007, India.
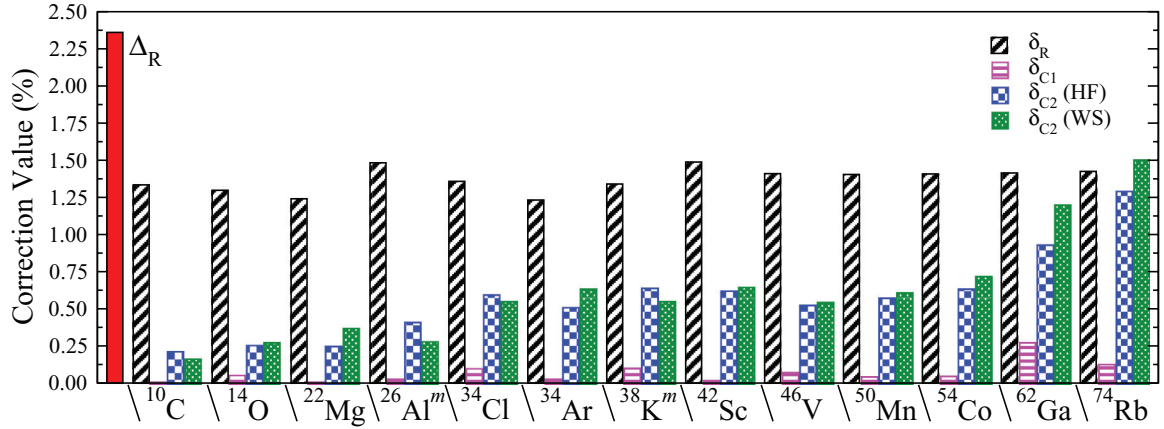
FIG. 1. (Color online) A nucleus-by-nucleus comparison of the theoretical corrections in Eq. (1). The two δ_{C2} values for each case arise from the Woods-Saxon (WS) and Hartree-Fock (HF) treatment of the radial wave functions in the radial-overlap part of the ISB correction. The values included are taken from Refs. [1,3].

Since these revisions were published, there has been a relative explosion of work on the δ_C corrections, including critiques of the existing formalism [6,7], approaches using density functional theory [8] and relativistic random phase approximation (RPA) [9], analyses based on the isovector monopole resonance [10,11], and global analyses of the available δ_C calculations [12,13] using some of the techniques originally pioneered by Wilkinson [14]. Some of these calculations have resulted in significantly different δ_C values, which consequently shift the extracted mean value of $\mathcal{F}t$ significantly. Although these new techniques have addressed some important concerns, none have yet achieved the same level of refinement required for Standard-Model tests as those of Towner and Hardy [1–3]. In fact, the calculations have been thoroughly tested for two $A = 32$ nuclei [15,16] where the corrections are large, and are in excellent agreement with the experimentally extracted δ_C values.

Since the extraction of $V_{\rm ud}$ and the test of the conserved-vector-current (CVC) hypothesis are heavily dependent on these ISB calculations, experimental tests of the validity of the shell-model calculations using the modified surface-δ, GXPF1, and GXPF1a interactions, as well as different truncation schemes, are required. For this purpose, a program of single and two-nucleon transfer reactions has been initiated. This paper reports a measurement of the $^{64}{\rm Zn}(\vec{d}, t)^{63}{\rm Zn}$ reaction, the first experiment in this program.

A. Towner and Hardy δ_C calculations

The ISB correction is used to correct the exact-symmetry matrix element, M_0, to obtain the Fermi-transition matrix element, M_F:

$$|M_F|^2 = |M_0|^2(1 - \delta_C). \tag{2}$$

The theoretical approach of Towner and Hardy (TH) [1,3] uses a separation of δ_C into a sum of two terms:

$$\delta_C \approx \delta_{C1} + \delta_{C2}, \tag{3}$$

where δ_{C1} is the ISB correction due to different configuration mixing between the parent and daughter states in the

superallowed decay, and δ_{C2} results from an imperfect radial overlap between the initial and final spatial nuclear wave functions. The isospin-mixing portion of the ISB correction is by far the smaller of the two terms and can be directly probed through the observation of nonanalog β-decay branching ratios to excited 0^+ states in the individual superallowed β-decay systems [17]:

$$\delta_{C1}^n \approx \left(\frac{f_0}{f_n}\right) B_n \frac{(1 - \delta_{C1})}{B_0} \approx \left(\frac{f_0}{f_n}\right) B_n, \tag{4}$$

where f_0 and f_n are the phase-space factors for decay to the ground state and the nth excited 0^+ state, respectively. The formalism associated with the calculation of the isospin-mixing correction term is described in detail in Refs. [3,5].

Due to the large relative contribution to the overall δ_C correction, δ_{C2} has garnered most of the recent attention, including the inclusion of specific core orbitals into the model space used in the calculation for some nuclei. Due to the importance of the δ_{C2} term on the resulting ISB correction values, experimental tests of the calculations are required. The work presented here focuses entirely on this radial-overlap term in the correction.

The contributions to these radial-overlap correction terms are related to the single-nucleon transfer spectroscopic factors via [3]

$$\delta_{C2} \approx \sum_{\pi^<,\alpha} S_\alpha^< \Omega_\alpha^< - \frac{1}{2} \sum_{\pi^>,\alpha} S_\alpha^> \Omega_\alpha^>, \tag{5}$$

where $S^{<,>}$ is the spectroscopic factor for the pickup of a neutron in orbital α, and π is the state in the final nucleus, $^{63}{\rm Zn}$, with $\pi^<$ being states with lower isospin, $T_\pi = 1/2$, and $\pi^>$ being states of higher isospin, $T_\pi = 3/2$. Further, $\Omega_\alpha^{<,>}$ is the radial mismatch factor for the respective states, and these are calculated on an orbital-by-orbital basis, as described in Ref. [3]. The sum extends over all states π in the final $(A - 1)$ nucleus. The spectroscopic factors used in the evaluation of δ_{C2} are calculated within the defined shell-model space; however, the orbitals of importance to be included in this calculation are chosen based on experimental observations. Specifically, if the
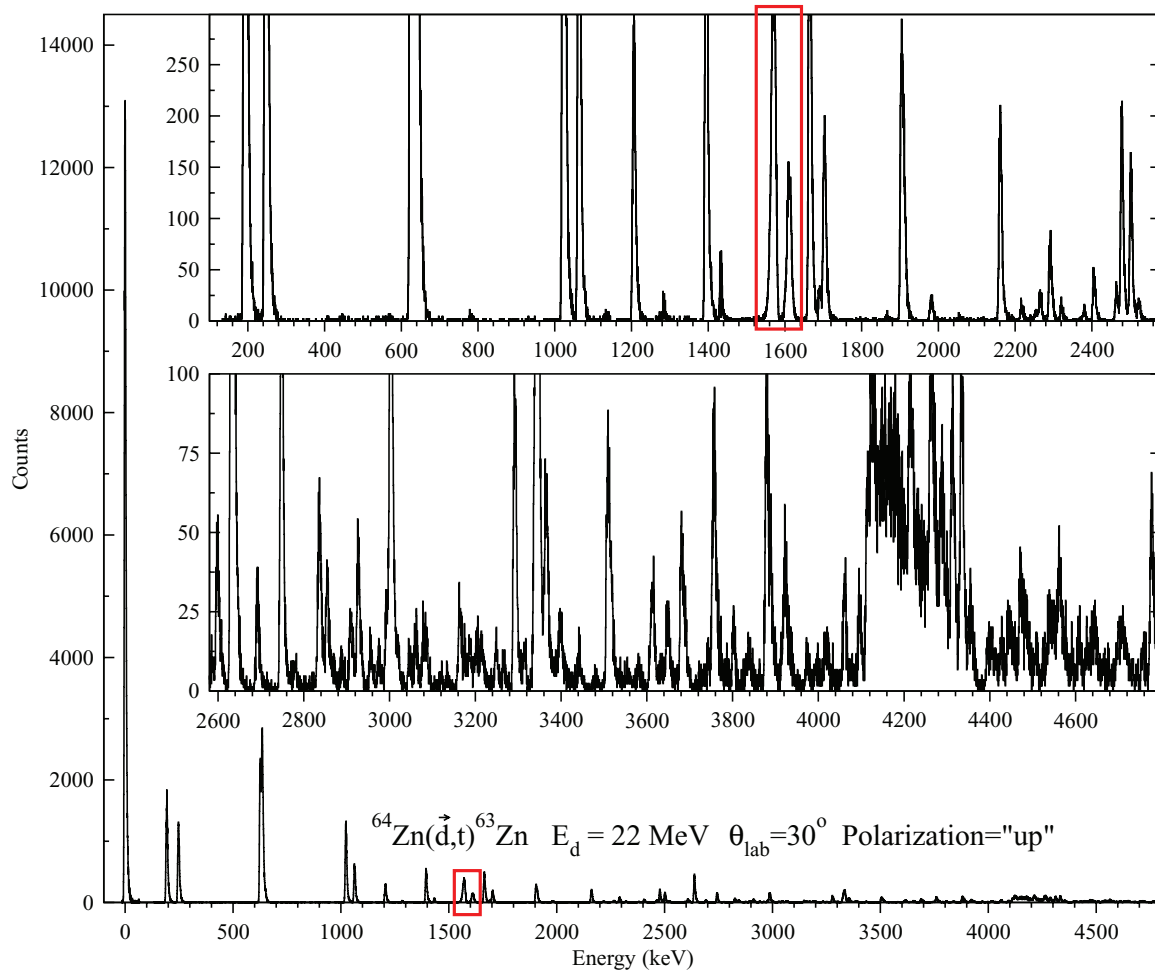
FIG. 2. (Color online) Complete spectrum of observed tritons in this experiment at $\theta_{\text{lab}} = 30°$ resulting from 22-MeV "up" polarized deuterons on 99.3(1)% ^{64}Zn. Experimental limitations required states from 3.8 to 4.8 MeV to be shown at $\theta_{\text{lab}} = 25°$. In order to appropriately show the individual level detail, two inset panels are expanded on the regions of (i) 100–2580 keV and (ii) 2580–4800 keV, respectively. The wide feature at ∼4.1–4.3 MeV is the result of observing tritons from a ($\vec{d}, t$) reaction on oxygen or carbon in the target. The two peaks shown within the red box near 1.6 MeV result from ($\vec{d}, t$) transfer from a similar mass impurity within the target, as discussed in the text, and thus are not states in ^{63}Zn.

orbital has a spectroscopic strength of >0.5 it is included in the calculation space. For the case of ^{62}Ga superallowed β decay, the most important core-orbital contribution is due to particles in the $f_{7/2}$ shell; however, the relevant $f_{7/2}$ experimental spectroscopic information does not exist. The calculations of Ref. [3] nonetheless included the possibility of opening one hole in the $\nu f_{7/2}$ shell.

Although the use of experimental spectroscopic factors has been criticized due to their nonobservable nature [18], it has been shown [19] that although the spectroscopic factors are not strict quantum observables, the results gained from these experimental values are in fact self-consistent, and provide an excellent reference for comparison to theory.

B. Experimental motivation for the study of ^{64}Zn($\vec{d}, t$)

The experimental ft value for ^{62}Ga, with a fractional uncertainty of $<0.05\%$ [1], has a precision approaching those

of the best cases in the sd shell [20]. However, detailed studies [21,22] of the nonanalog Fermi β-decay branches of ^{62}Ga $\rightarrow$ ^{62}Zn have shown discrepancies with theory and called into question the truncations of the shell-model space used for the ISB corrections in the $A \geqslant 62$ nuclei. Experimental guidance for the applied ISB corrections in this mass region is thus crucial. For lighter superallowed systems, light-ion beams on stable targets can be used to access the states required for these calculations. However, the nuclear system relevant for the ^{62}Ga calculations (^{62}Zn $\rightarrow$ ^{61}Zn) requires a transfer reaction in inverse kinematics using radioactive ion beams (RIBs), which creates some experimental challenges. These limitations include: (i) a difficulty to achieve the required final-state energy resolution, (ii) the requirement of a polarized target to obtain final-state J values, and (iii) relatively low RIB intensities causing prohibitively long experiment times. To circumvent these challenges, the relevant orbital strengths can be tested in the closest stable system, ^{64}Zn $\rightarrow$ ^{63}Zn, where access to transfer reactions on a heavy, stable target are possible. In

TABLE I. Optical model parameters for 22-MeV polarized $^{64}Zn(\vec{d}, t)^{63}Zn_{g.s.}$. The optimal deuteron [30] and triton [33] sets were chosen for their suitability in reproducing their respective elastic scattering data, as outlined further in Sec. III A. Global parameters provide expressions as a function of particle energy, and therefore the respective triton parameters change slightly for transfers into excited states of ^{63}Zn.

Parameter	Deuteron	Triton
V_v (MeV)	91.243	168.371
r_v (fm)	1.150	1.082
a_v (fm)	0.769	0.759
W_v (MeV)	2.472	13.013
r_v (fm)	1.330	1.276
a_v (fm)	0.455	1.195
W_s (MeV)	10.157	24.240
r_s (fm)	1.372	1.135
a_s (fm)	0.779	0.858
V_{so} (MeV)	3.557	1.9029
r_{so} (fm)	0.972	0.502
a_{so} (fm)	1.011	0.147
r_c (fm)	1.303	1.422

order for an appropriate comparison to theory, spectroscopic factor calculations for the $^{64}Zn \rightarrow {}^{63}Zn$ were also carried out, using the same prescriptions as Refs. [3,5], and are discussed in Sec. V, along with independent calculations performed using a larger shell-model space.

II. EXPERIMENT

The experiment was performed at the Maier-Leibnitz-Laboratorium (MLL) of Ludwig-Maximilians-Universität (LMU) and Technische Universität München (TUM) in Garching, Germany. Using a 22-MeV polarized deuteron beam from the MP tandem Van de Graaff accelerator and the Stern-Gerlach polarized ion source [23], polarized deuterons were incident on a 99.3(1)% isotopically pure, 126(6) μg/cm^2 ^{64}Zn target with a 13 μg/cm^2 carbon backing. The reaction products were momentum analyzed using a Q3D magnetic spectrograph, and the resulting particles were detected at the focal plane [24]. The target thickness was experimentally determined through a normalization of the experimental deuteron elastic scattering cross section to the distorted-wave Born approximation (DWBA) prediction at 15°, described below, where it is nearly pure Coulomb scattering.

By using 22-MeV incident deuterons, polarized to $p = 80(4)\%$, and beam currents up to $\sim$1 μA, a single-neutron pickup reaction experiment was performed using the Q3D spectrometer at nine angles between 10° and 60°. Five momentum settings of the spectrograph were taken at each angle to cover excitation energies up to 4.8 MeV, with both polarizations. A 0° Faraday cup inside the target chamber was used to determine the number of beam particles incident on the ^{64}Zn target by integrating the total current. This information, along with the data-acquisition system (DAQ) dead time, was read into the data stream using scalers. Dead time associated with the detector was also tracked, where all events gathered while the system was dead were binned in channel zero of each respective particle-energy spectrum. These dead-time values were typically $\leqslant$0.5% and $\sim$1%–22% for the detector and DAQ, respectively.

The focal-plane detector consists of two proportional counters that provide ΔE information, one of which has a position-sensitive cathode strip, and a thick plastic E detector. Particle identification is achieved via ΔE-ΔE and ΔE-E information. The observed triton spectrum at $\theta_{lab} = 30°$ is
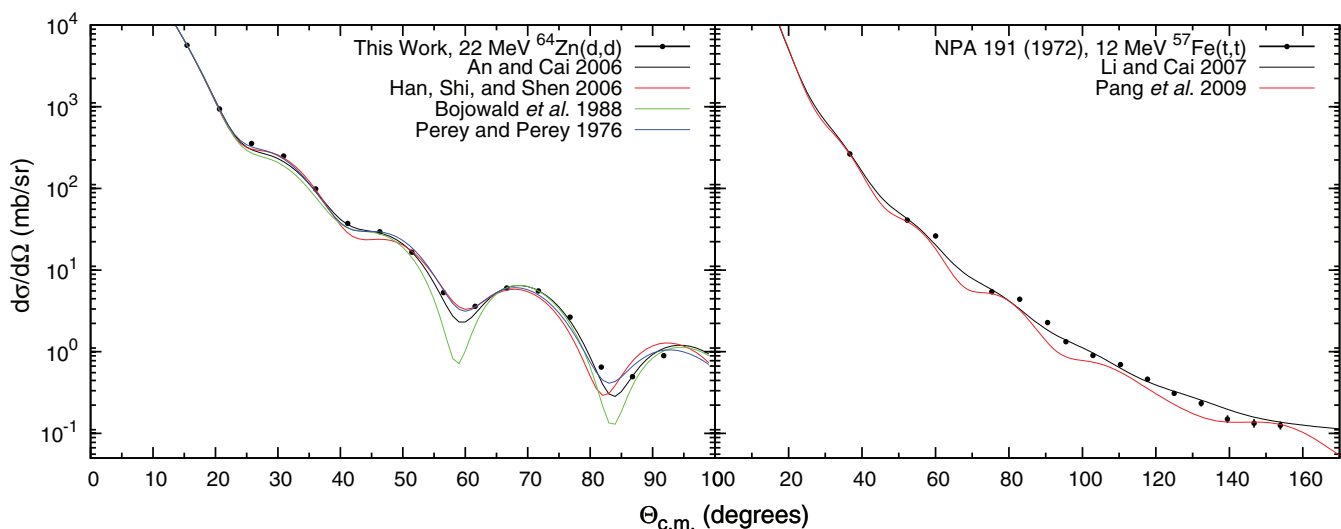
FIG. 3. (Color online) Comparison of several global triton and deuteron OMP sets to experimental elastic scattering data of 22-MeV deuterons on ^{64}Zn (left) and 12-MeV tritons on $^{57}Fe(t, t)$ [32] (right). All of the global OMP sets presented provide reasonable reproduction of the data; however, the optimal sets were determined to be those of An and Cai [30] and Li, Liang, and Cai [33] for deuterons and tritons, respectively. Experimental errors are shown; however, in most cases, they are smaller than the data points.
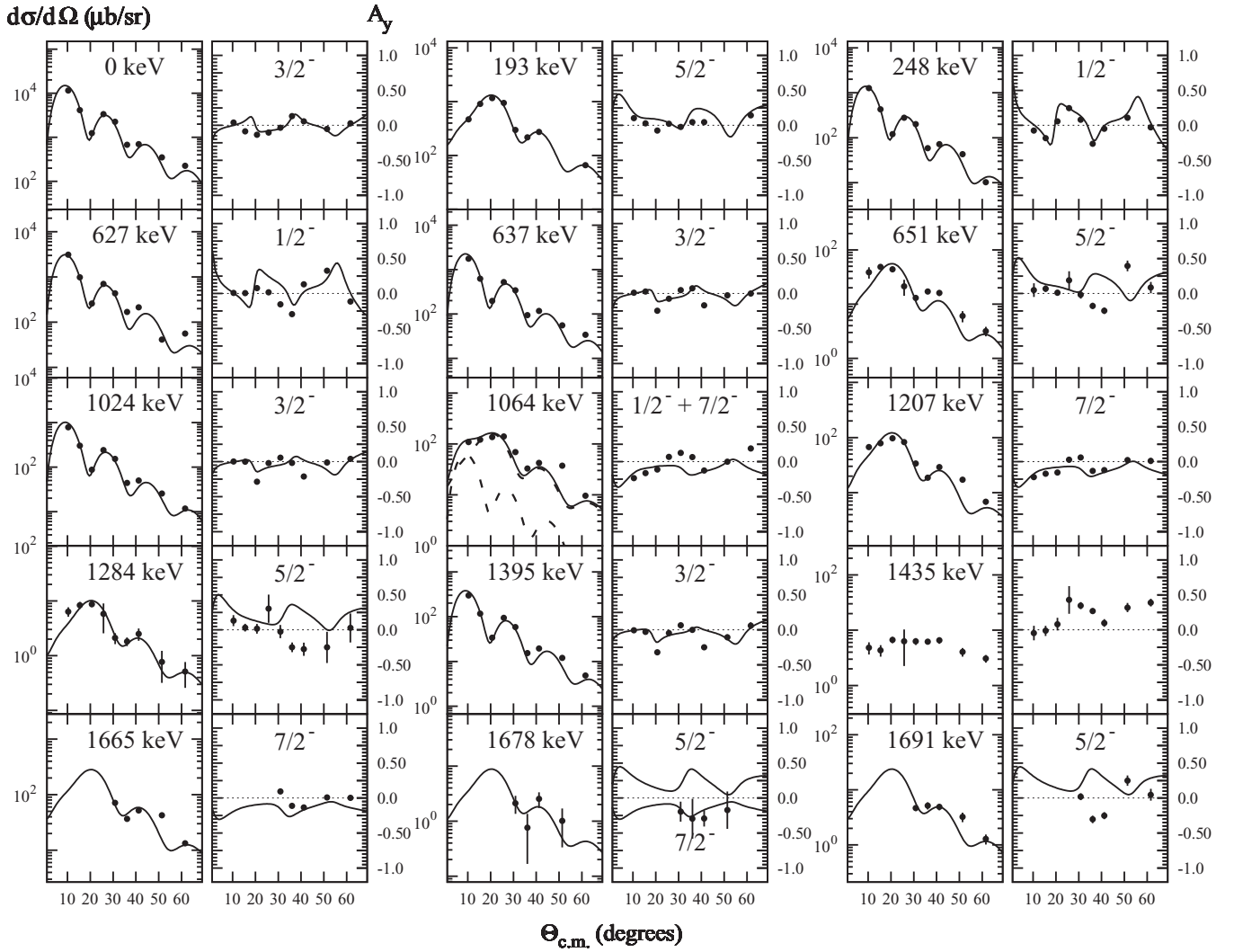
FIG. 4. Angular distributions and vector analyzing powers for states populated in ^{63}Zn from 0.0 to 1.7 MeV. The curves are a result of DWBA calculations, described in the text, for the various j^π transfers indicated. The states with known $I^\pi = 5/2^-$ are shown with the $J = 5/2$ curves, despite the generally poor agreement with the vector analyzing power data. For the doublet at 1064 keV, the dashed curves represent the respective $L = 1$ and $L = 3$ components of the angular distribution, and the solid line shows the total. The 1435-keV state is shown with no curves, since the population of this $9/2^-$ state cannot be described by the one-step DWBA calculations for this reaction. Broad peaks in the spectrum at 1.6–1.9 MeV caused by light target impurities result in missing cross-section data for these states from $10°$ to $25°$. The state at 1435 keV is evaluated as a $9/2^-$ state in Ref. [25]. Other states of this nature were observed in this work and are described further in Sec. IV A.

displayed in Fig. 2. The typical resolution obtained for the particle energy spectra was ~8 keV full width at half maximum (FWHM).

A. Target impurities

Careful attention was paid to reducing the possibility of level misidentification from impurities in the target. For target impurities which have very different masses (^{16}O, ^{12}C, etc.), the kinematic broadening of the peaks on the focal plane of the Q3D prevents a misidentification. However, because the peaks are so broad, they overwhelm the spectrum at certain angles, which causes gaps in the plotted angular distributions. To circumvent this, the momentum settings were varied slightly

as a function of angle in cases where the peaks could be shifted out of the spectrum. As a result, states from ~1.6–1.9 MeV do not contain cross-section data from $10°$ to $25°$. An example of the target impurity, as observed on the Q3D focal plane, can be seen at ~4.3 MeV in Fig. 2.

Since the kinematic dependance of the Q3D is reaction specific, an examination of the peak position as a function of angle was performed, for each momentum setting, to eliminate observed reactions on isotopic and other similar-mass impurities. The two peaks highlighted in Fig. 2 were the only observed peaks that systematically shifted as a function of angle, and were thus removed from the analysis. For the $<1\%$ isotopic target impurities of ^{68,66}Zn, the reaction Q-value differences put the ground-state transfers into ^{67,65}Zn below
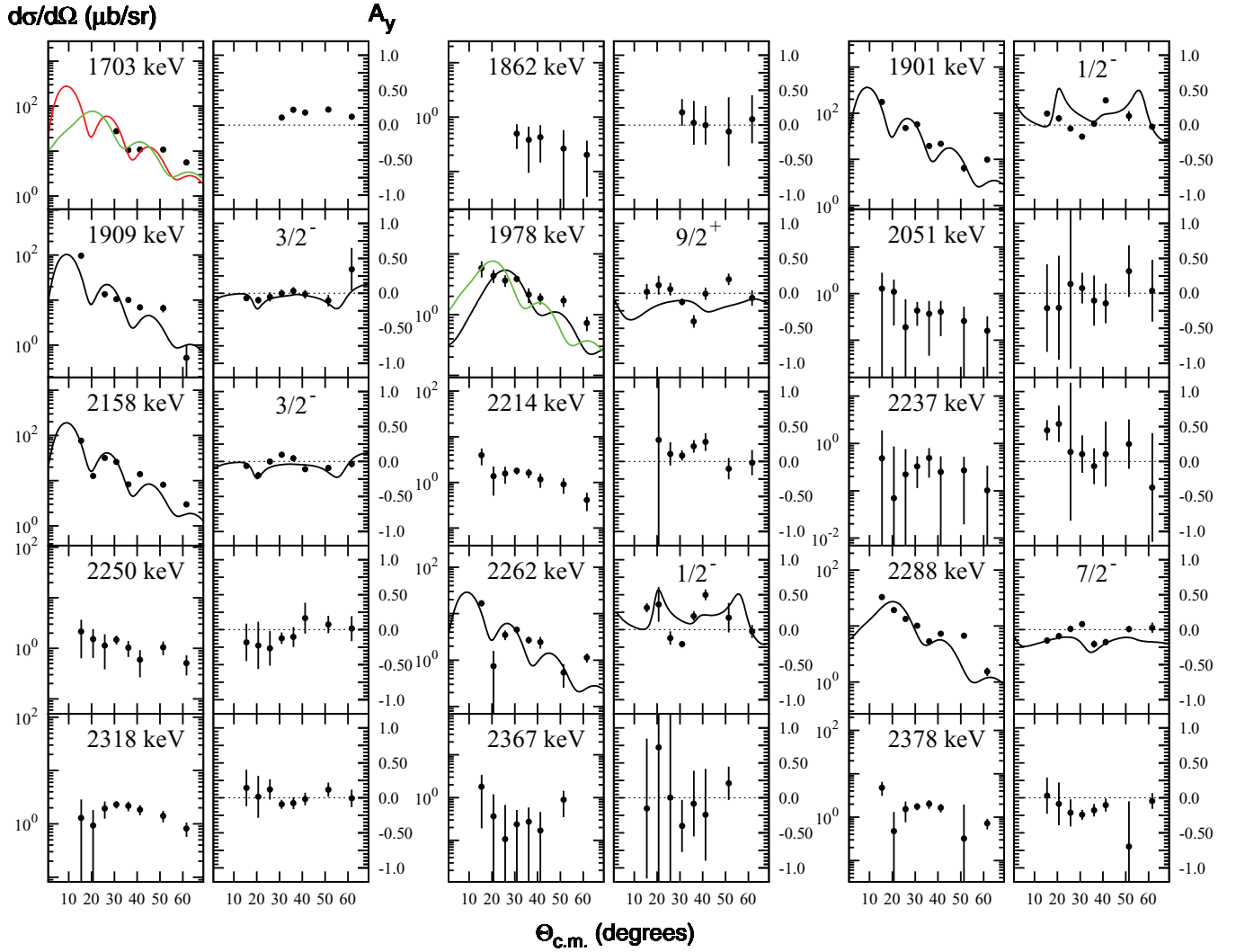
FIG. 5. (Color online) Angular distributions and vector analyzing powers for states populated in ^{63}Zn from 1.7 to 2.4 MeV. For some levels, 10° data are not present due to large backgrounds caused by scattered beams within the target chamber. For states where multiple L transfers are able to describe the data, both $L = 1$ (red) and $L = 3$ (green) DWBA calculations are shown. The state at 1978 keV is suggested here as populated in an $L = 4$ (black) transfer; however, the $L = 3$ (green) curve is also displayed with the data, for comparison.

channel 0 and were therefore outside the observed momentum range. In addition, no excited-state peaks from these impurities were observed at the expected energies.

B. Energy calibration

Many of the levels presented in this work have not previously been observed. As a result, a careful examination of the energy dependence of the Q3D focal plane was conducted and extrapolated to energies above ∼3 MeV. By using states in ^{63}Zn with well-determined energies from γ-ray work [25], an expression for the nonlinearity of the Q3D focal plane as a function of outgoing triton energy was determined. In order to help constrain the calibration where known levels were sparse, a secondary ^{54}Fe target [96.81(5)% enriched] was used as a reference for energy calibration of the magnetic spectrograph, using the $(\vec{d}, t)$ reaction. Triton energy losses through the target

(and backing) were ∼4 keV, and this loss was accounted for in the calibration. The combination of known ^{63}Zn and ^{53}Fe levels from 0 to ∼3.5 MeV were used to develop an expression for the quadratic term in the focal plane calibration. Once this expression was determined, a second-degree polynomial fit was conducted for each spectrum. The energy uncertainties increase for states above ∼3.5 MeV where calibration peaks were not available, and the focal-plane characterization is extrapolated.

C. Cross-section calculations

Differential cross sections were determined at each angle, for each momentum setting and polarization. These cross sections were calculated using (i) the integrated beam current at 0°, (ii) the total solid angle of the magnetic spectrograph (∼0.5–15 msr), (iii) the ^{64}Zn target thickness, (iv) system and
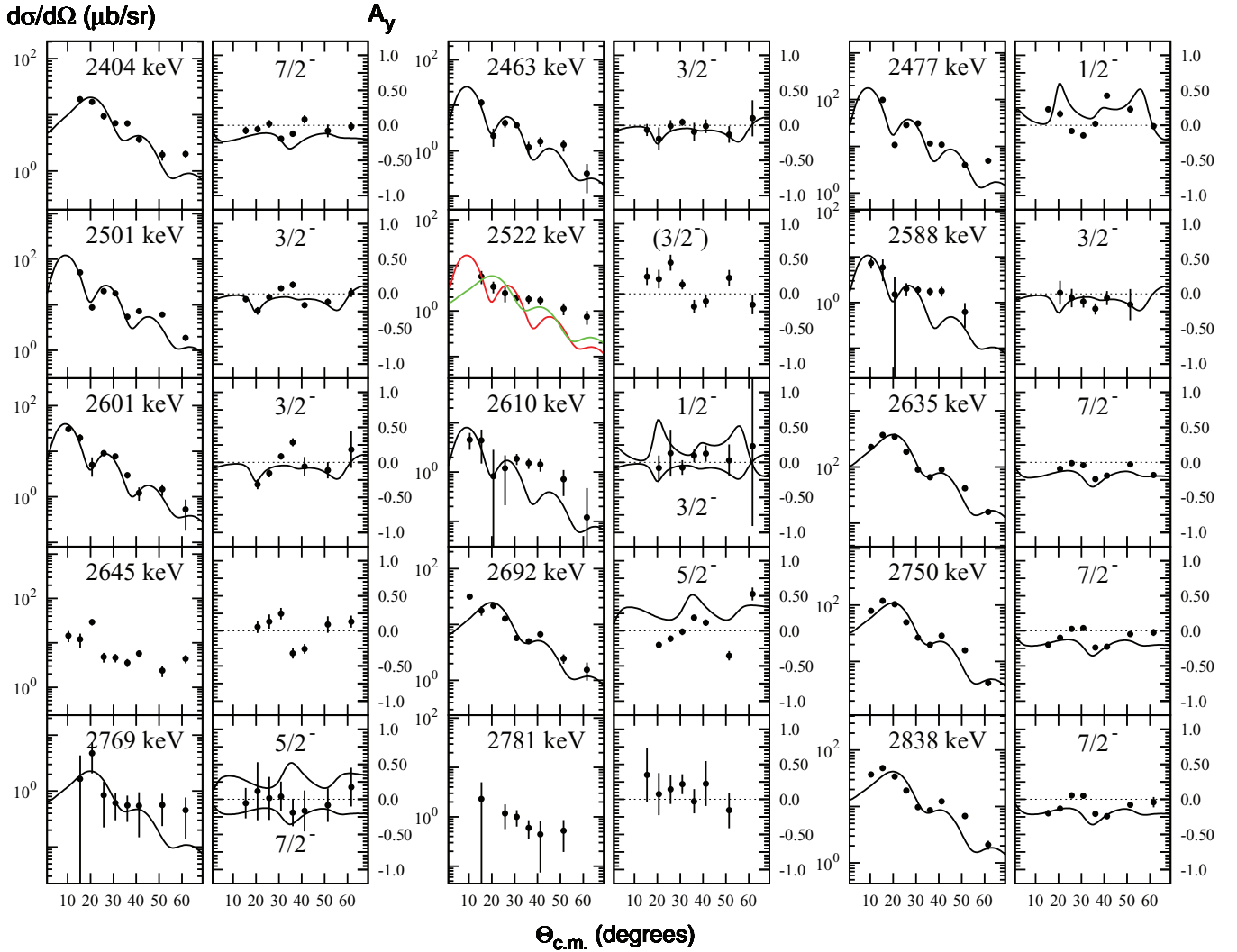
FIG. 6. (Color online) Angular distributions and vector analyzing powers for states populated in ^{63}Zn from 2.4 to 2.8 MeV. For states where multiple L transfers are able to describe the data, both $L = 1$ (red) and $L = 3$ (green) DWBA calculations are shown. The strongly populated state at 2635 keV represents the single largest source of $1f_{7/2}$ strength of all the states observed in this work.

detector dead times, and (v) the respective peak areas from the various energy spectra. By using the complete set of measured cross sections, angular distributions were constructed for all levels observed in ^{63}Zn and are discussed in Sec. IV.

As a result of the polarization of the incoming deuteron beam, cross-section asymmetries were also calculated as

$$A_y = \frac{2}{3p} \frac{\frac{d\sigma}{d\Omega}\uparrow - \frac{d\sigma}{d\Omega}\downarrow}{\frac{d\sigma}{d\Omega}\uparrow + \frac{d\sigma}{d\Omega}\downarrow}, \qquad (6)$$

where $\frac{d\sigma}{d\Omega}\uparrow$ and $\frac{d\sigma}{d\Omega}\downarrow$ are the measured cross sections for incident deuterons with "up" and "down" polarization, respectively, and $p = 80(4)\%$ is the polarization efficiency of the Stern-Gerlach source [23].

A 5% systematic uncertainty was combined in quadrature with the other experimental and statistical uncertainties to account for differences in the measured target thickness. For the more precisely determined cross sections, this becomes the limiting uncertainty.

III. DWBA CALCULATIONS AND EXTRACTED SPECTROSCOPIC FACTORS

Assessing the accuracy of respective theoretical shell-model interactions requires a comparison to experimental spectroscopic data. The spectroscopic information relevant to these comparisons are level energies, I^π values, and spectroscopic factors. Experimentally, the spectroscopic factors are determined by a normalization of the theoretical single-particle predictions provided by a DWBA calculation. This normalization yields the C^2S value,

$$\frac{d\sigma}{d\Omega}\bigg|_{\exp} = C^2S \cdot \frac{N}{(2J+1)} \cdot \frac{d\sigma}{d\Omega}\bigg|_{\text{DWUCK4}}, \qquad (7)$$

where J is the angular momentum of the transferred particle and $N = 3.33$ for a (d,t) reaction as recommended in Ref. [26]. The work reported here uses zero-range DWBA calculations carried out using the University of Colorado DWUCK4 software package [26]. For the purposes of these
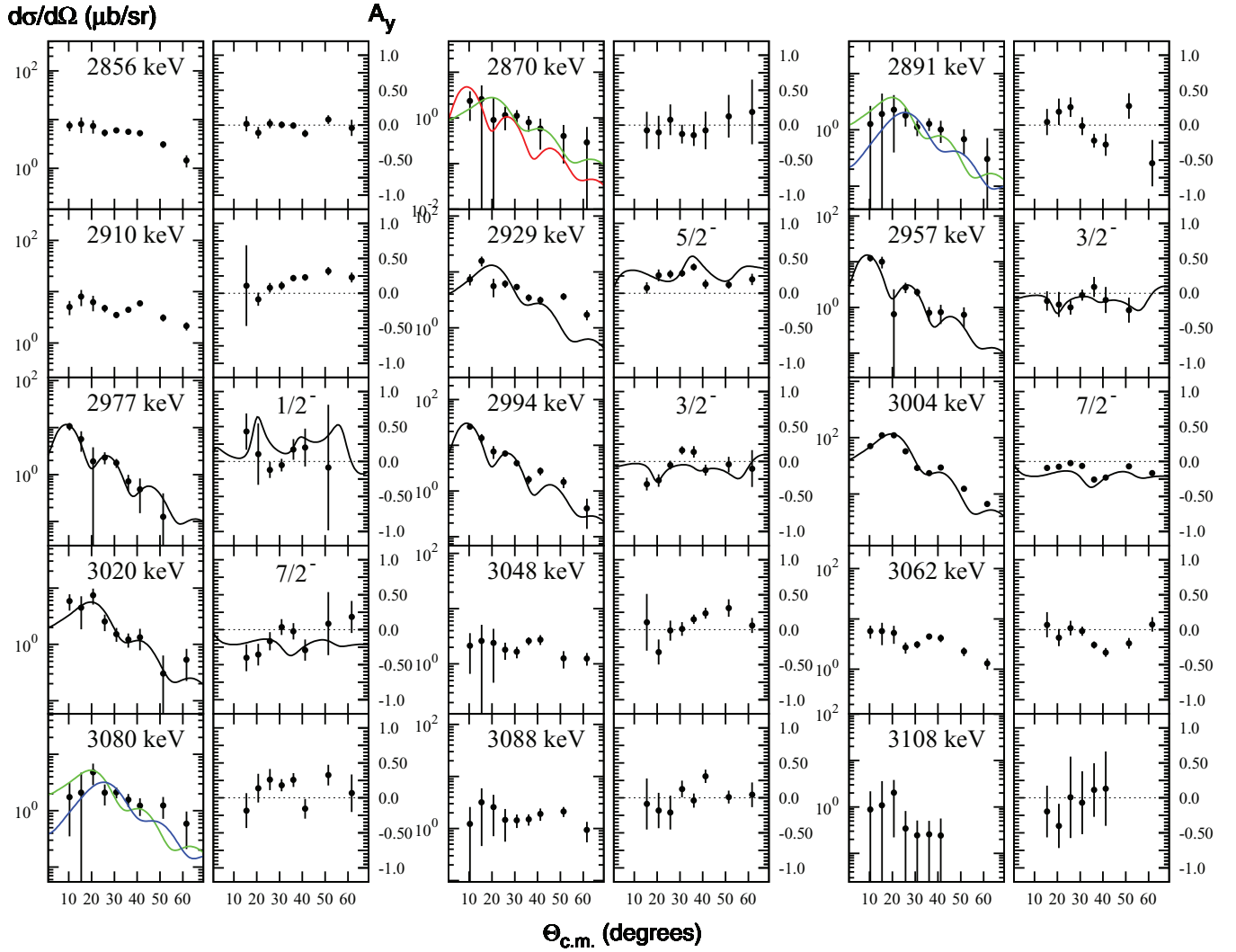
FIG. 7. (Color online) Angular distributions and vector analyzing powers for states populated in ^{63}Zn from 2.9 to 3.1 MeV. For states where multiple L transfers are able to describe the data, $L = 1$ (red), $L = 3$ (green), and $L = 4$ (blue) DWBA calculations are shown.

calculations, the optical potential for the Born-approximation calculation is

$$V(r) = -V_{\mathrm{v}} f_r(r) - i\,W_{\mathrm{v}} f_{\mathrm{v}}(r) + i4W_{\mathrm{s}} a_{\mathrm{s}} \frac{df_{\mathrm{s}}(r)}{dr}$$
$$+ \lambda_{\pi}^2 \frac{V_{\mathrm{so}} + W_{\mathrm{so}}}{r} \frac{df_{\mathrm{so}}(r)}{dr} \vec{\sigma} \cdot \vec{\lambda} + V_C(r), \qquad (8)$$

where

$$V_C(r) = \frac{ZZ'e^2}{r} \quad \text{for} \quad r \geqslant R_{\mathrm{c}}$$
$$= \left(\frac{ZZ'e^2}{2R_{\mathrm{c}}} \right) \left(3 - \frac{r^2}{R_{\mathrm{c}}^2} \right) \quad \text{for} \quad r \leqslant R_{\mathrm{c}}, \qquad (9)$$

and where $R_{\mathrm{c}} = r_{\mathrm{c}} A^{1/3}$, with $i = \mathrm{v}$ (volume), s (surface or volume-derivative), or so (spin-orbit).

The DWBA calculation results are heavily dependent on the incoming and outgoing channels of the reaction, which therefore requires appropriate optical-model parameters (OMPs) for the deuteron and triton at this mass and energy. The selection criteria for the global triton and deuteron OMP sets used in the analysis of this work are discussed in Sec. III A. In an attempt to handle some of the model-dependent uncertainties which arise from the extraction of the spectroscopic factors, all of the global sets outlined below are used to examine these effects. This analysis is described in detail in Sec. III B. The final DWUCK4 calculations employed both nonlocal and finite-range corrections, as recommended in Ref. [26] for (d, t) reactions.

A. Choice of optical model parameters

In order to test the validity of the various global OMPs available in the literature for deuterons and tritons, a comparison
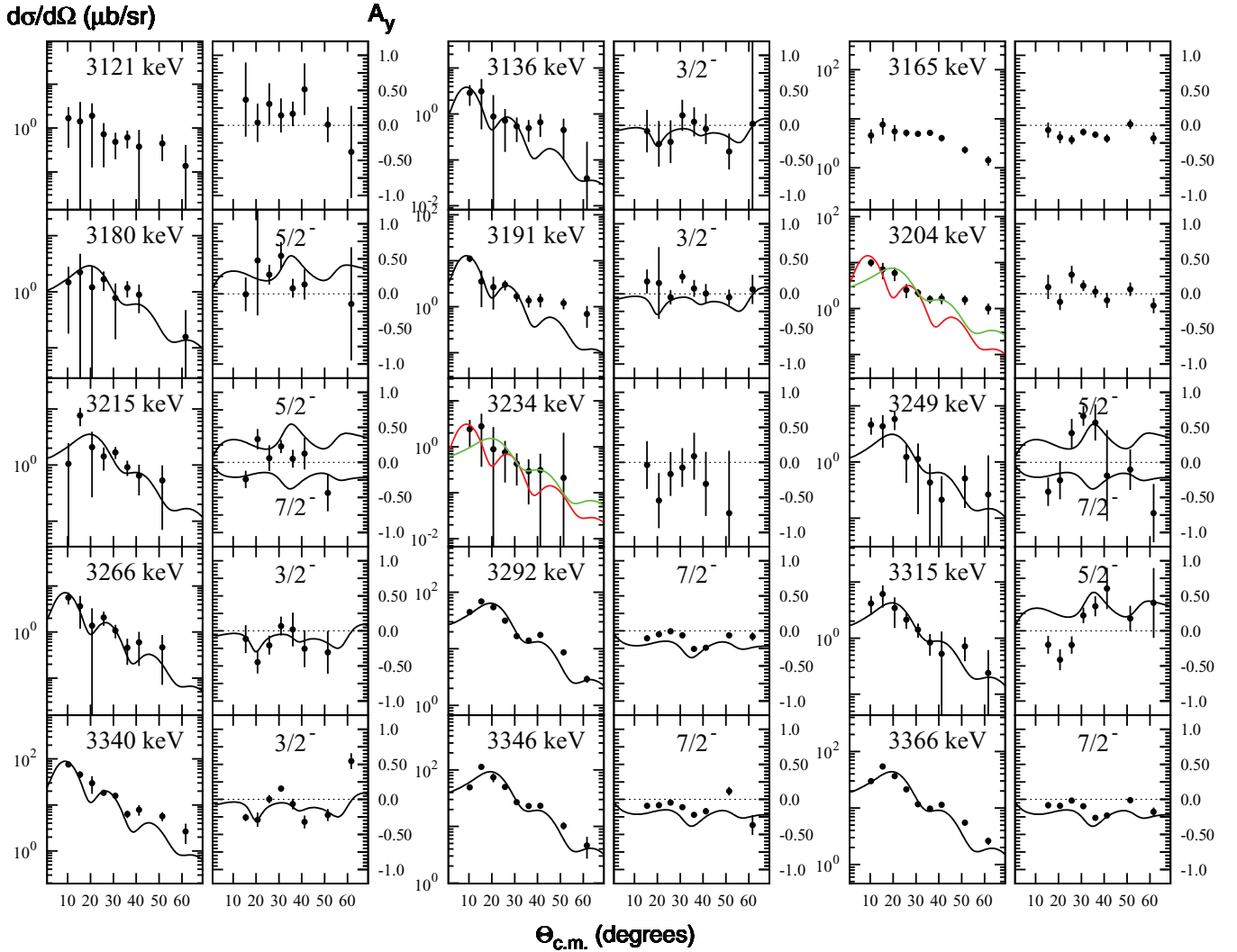
FIG. 8. (Color online) Angular distributions and vector analyzing powers for states populated in ^{63}Zn from 3.1 to 3.4 MeV. For states where multiple L transfers are able to describe the data, both $L = 1$ (red) and $L = 3$ (green) DWBA calculations are shown.

of observed elastic scattering data to the calculated DWBA curves was made.

1. Deuteron

An investigation of 22-MeV polarized deuteron elastic scattering from ^{64}Zn was performed following the single-neutron transfer experiment, and a comparison of the available global OMP sets was conducted to determine their suitability for 22-MeV deuterons on ^{64}Zn. The four global sets tested were those of Perey and Perey [27], Bojowald *et al.* [28], Han, Shi, and Shen [29], and An and Cai [30]. The comparison showed that all four sets did an excellent job reproducing the elastic scattering data; however, the set of An and Cai was chosen as the optimal set due to an outstanding agreement with both the vector analyzing powers and elastic scattering angular distribution. The global OMP values calculated for 22-MeV deuterons on ^{64}Zn are given in Table I, and the comparison of the calculated angular distributions to the data is shown in Fig. 3.

2. Triton

For the outgoing reaction channel, experimental triton elastic scattering data are not directly available. Therefore, an examination of the published data closest to the energy and mass range required here ($Z = 30$, $A = 63$, and $E = 16.4$–11.6 MeV) was performed. By using the Experimental Nuclear Reaction Data (EXFOR) database [31], cross sections for 12-MeV triton elastic scattering on ^{57}Fe were found to be the closest available set of experimental data [32]. Fewer triton OMP sets are available; however, the chosen sets for comparison here are those of Li, Liang, and Cai [33] and Pang *et al.* [34]. A comparison of the two global triton OMP sets to the experimental data was performed and is displayed in Fig. 3, and from this analysis, the optimal triton OMP set was determined to be that of Li, Liang, and Cai [33]. The calculated parameters from the global set for 16.4-MeV tritons are given in Table I.

When excited states in ^{63}Zn are probed, the outgoing triton is lower in energy by the amount of excitation within the
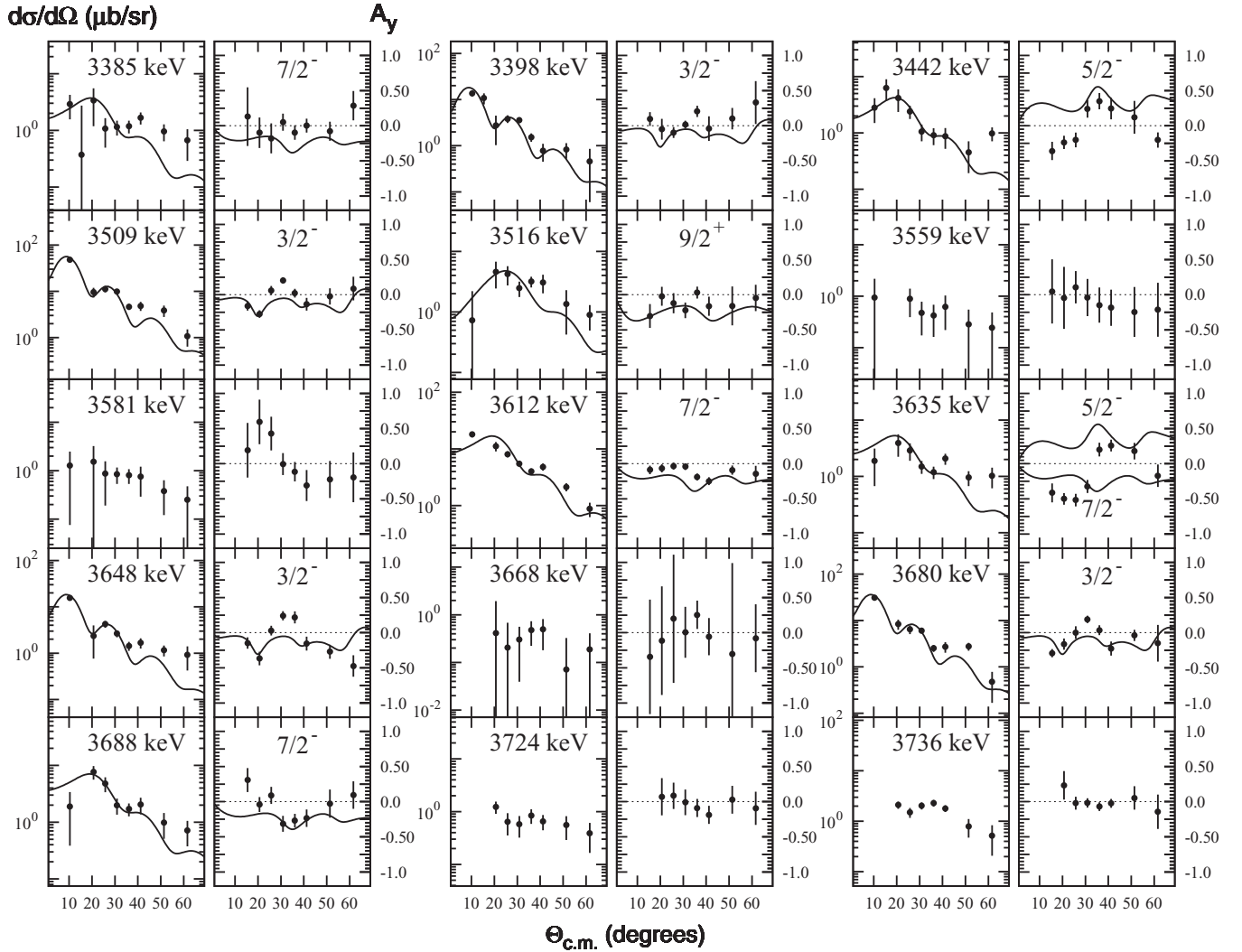
FIG. 9. Angular distributions and vector analyzing powers for states populated in ^{63}Zn from 3.4 to 3.7 MeV.

nucleus; therefore the parameters are dynamically calculated for each state. This process changes the calculated angular distributions only slightly for states in ^{63}Zn up to 5 MeV; however, the vector analyzing power shape and magnitudes do change significantly. By using the above optical-model parameters for deuterons and tritons, DWBA calculations for all observed states in ^{63}Zn were performed and compared to the experimental data shown in Figs. 4–14.

B. Experimental spectroscopic factors

For states where the transferred L was found but J could not be determined, both J transfer analyzing power curves are shown. For cases where neither J nor L could be determined, all three L curves are shown in the angular distribution panel; however, no A_y curves are shown in the vector analyzing power plots. For the states where J transfers were obtained, the individual level-by-level strength distribution is shown in Fig. 15.

1. Model dependencies of extracted spectroscopic factors

The uncertainty associated with the choice of global OMPs was examined by extracting the spectroscopic factors for the ground state and the first several excited state transfers using all combinations of deuteron and triton sets mentioned in Sec. III A. All eight combinations of OMP sets were used in the calculation of the ^{64}Zn$(\vec{d}, t)$ transfer for $L = 1, 3$, and 4. In all cases, these calculations resulted in $C^2 S$ values within 30% of those determined using the optimal sets of Refs. [30] and [33]. For the spectroscopic factors reported in Table II, only the 5% systematic and statistical uncertainties are summed in quadrature, to preserve the experimental information.

IV. DISCUSSION

A. Previously observed states

For certain states in ^{63}Zn that are tabulated in the evaluation of Ref. [25], a discussion of the agreement with the previous work is given in the following sections. Included in these
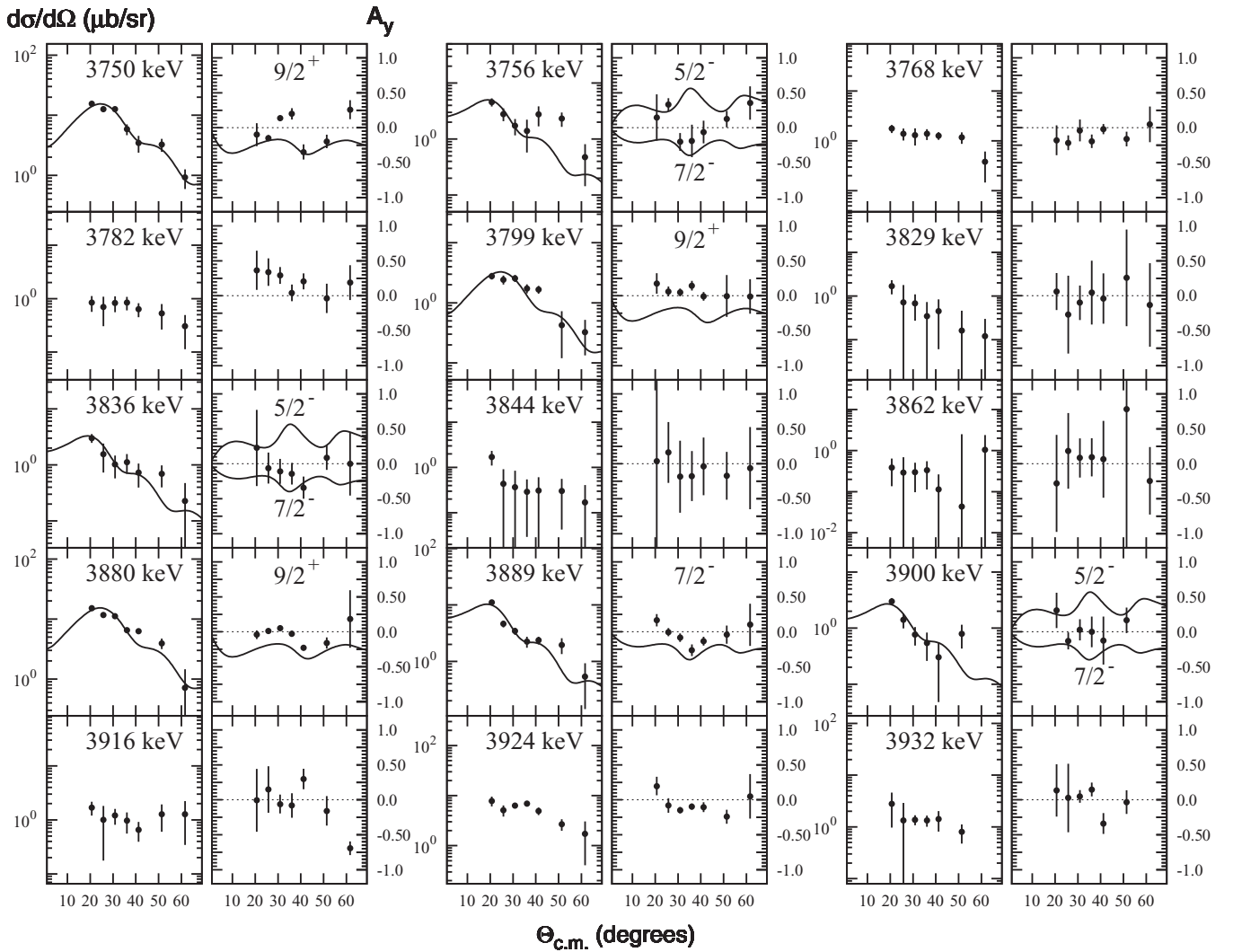
FIG. 10. Angular distributions and vector analyzing powers for states populated in ^{63}Zn from 3.8 to 3.9 MeV.

previous works are five single-neutron pickup experiments into ^{63}Zn, including a previous (d, t) experiment. In nearly all cases, the extracted spectroscopic factors from this work are lower than those from the other reactions; however, no uncertainties on the previous values were quoted. A state-by-state discussion and comparison for some of these levels is given below.

1. 3/2⁻ ground state

The normalized DWBA calculation shows excellent agreement with the data, confirming the previous assignment of a $3/2^-$ ground state. The literature values for $C^2S_{\text{g.s.}}$ are within 30% of each other, and all show general agreement with the value of 0.991(22) presented in this work.

2. 627-, 637-, and 650-keV triplet

The energy separation of these three levels is near the FWHM energy resolution of the current setup, thus providing an excellent test of the detection limit for this experiment. Due to the order of magnitude drop in cross section between

the 627 and 637-keV states and the 650-keV level, a fit of the latter yielded larger uncertainties. Continuing with the 650-keV state, the calculated A_{sy} curve for the $J = 5/2$ transfer does not reproduce the observed data as well as the other J transfers. However, the previously known 5/2 states display the same trend.

3. 1064-keV 1/2⁻ and 7/2⁻ unresolvable doublet

A doublet of known states at 1063.34(7) keV ($7/2^-$) and 1065.28(12) keV ($1/2^-$) [25] could not be separately resolved in this experiment due to their <2 keV energy difference and large cross-section variation. Therefore, a two-component fit was performed to the 1064-keV angular distribution data shown in Fig. 4 in order to extract the respective $1/2^-$ and $7/2^- C^2S$ values. The result of the fit, as well as both individual components, is shown with the angular distribution in Fig. 4. The result of this fit showed that the dominant component of the transfer is $J = 7/2$ (98%), with the $J = 1/2$ transfer only having an effect on the angular distribution at very low angles.
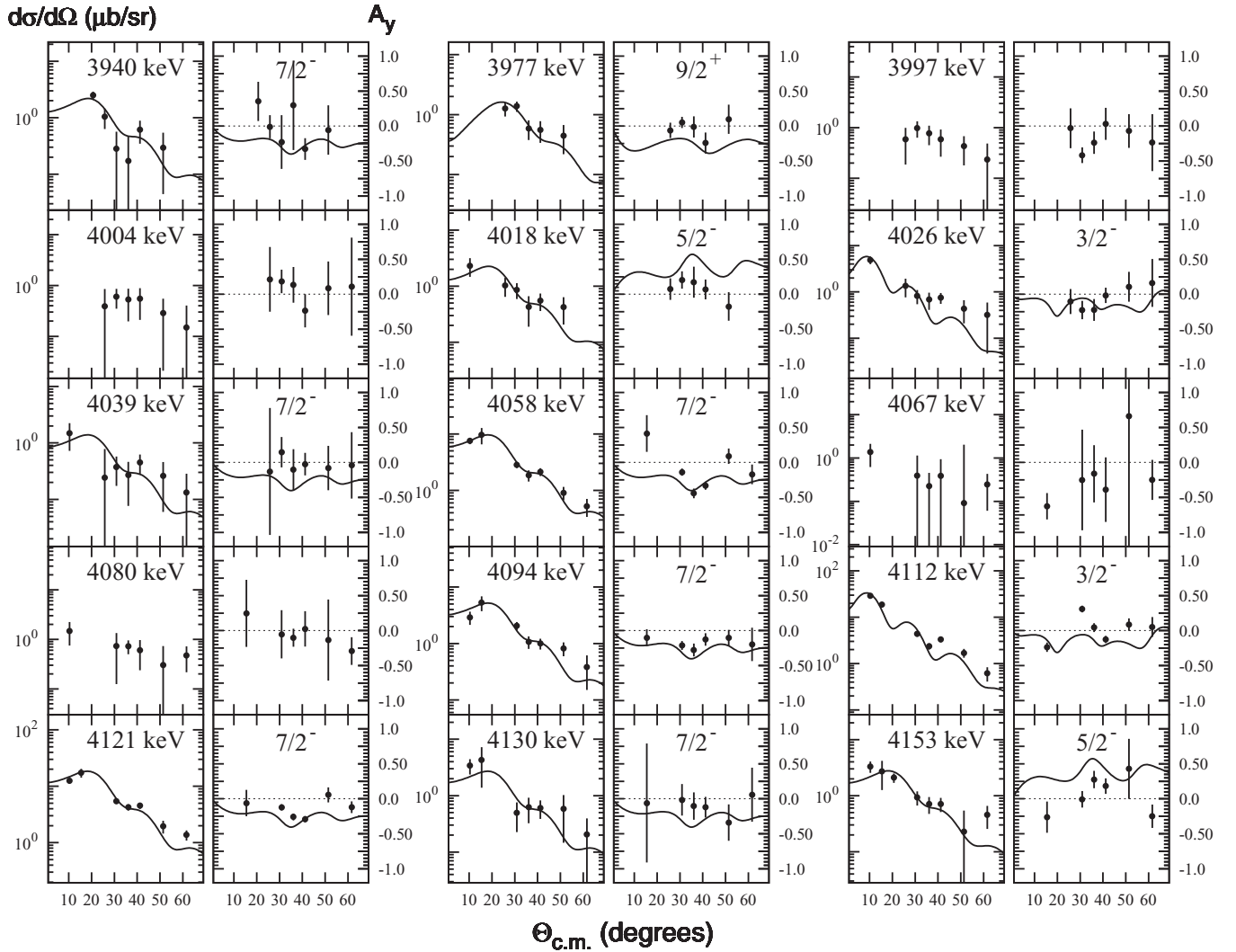
FIG. 11. Angular distributions and vector analyzing powers for states populated in ^{63}Zn from 3.9 to 4.2 MeV.

4. Unobserved 1420-keV state

Previous single-neutron transfer work performed using (d, t) and $(^3\text{He}, \alpha)$ reactions (Refs. [4,35,36]) report the observation of a 1420 keV $L = 1$ transfer that is not seen in this work. With the high sensitivity and resolution achieved in the present work, the likelihood of missing such a low-lying level is very low. Given this, and the fact that this level is not reported in any of the other evaluated works regarding ^{63}Zn, it is concluded that this level does not exist in ^{63}Zn.

5. 1435-keV state

The population of this level in ^{63}Zn is observed; however, the angular distribution does not reflect any of the possible L transfers expected. The evaluated I^π from Ref. [25] is $9/2^-$, which is not expected in this reaction without consideration of multi-step processes. This level has a previously observed enhanced $E2$ transition to the 193-keV state, and thus is interpreted as a $5/2^- \otimes 2_1^+$ state involving the ^{62}Zn 2_1^+ core.

Other states of this nature were observed in the present study as well, and are detailed in the discussion of the $9/2^-$ states below.

6. 1678-keV state

The lack of low-angle data (due to target impurities) for this state does not allow for a definite J^π assignment. An $L = 3$ transfer is suggested through the general agreement with the DWBA calculations shown in Fig. 4, and the nonobservation of this level in previous $(\alpha, n\gamma)$ work from Ref. [37] suggests a $5/2^-$ assignment. It is therefore concluded that this is a newly observed level.

7. 1703-keV state

Data in the literature include two states in this region: a $9/2^+$ state at 1703 keV from $(p, n\gamma)$ [38], $(\alpha, n\gamma)$ [39], and $^{50}\text{Cr}(^{16}\text{O}, 2pn\gamma)$ [40] work, and an $L = 3$ 1704-keV state only seen in $(^3\text{He}, \alpha)$ [4,35,36]. A 1691-keV state reported in the
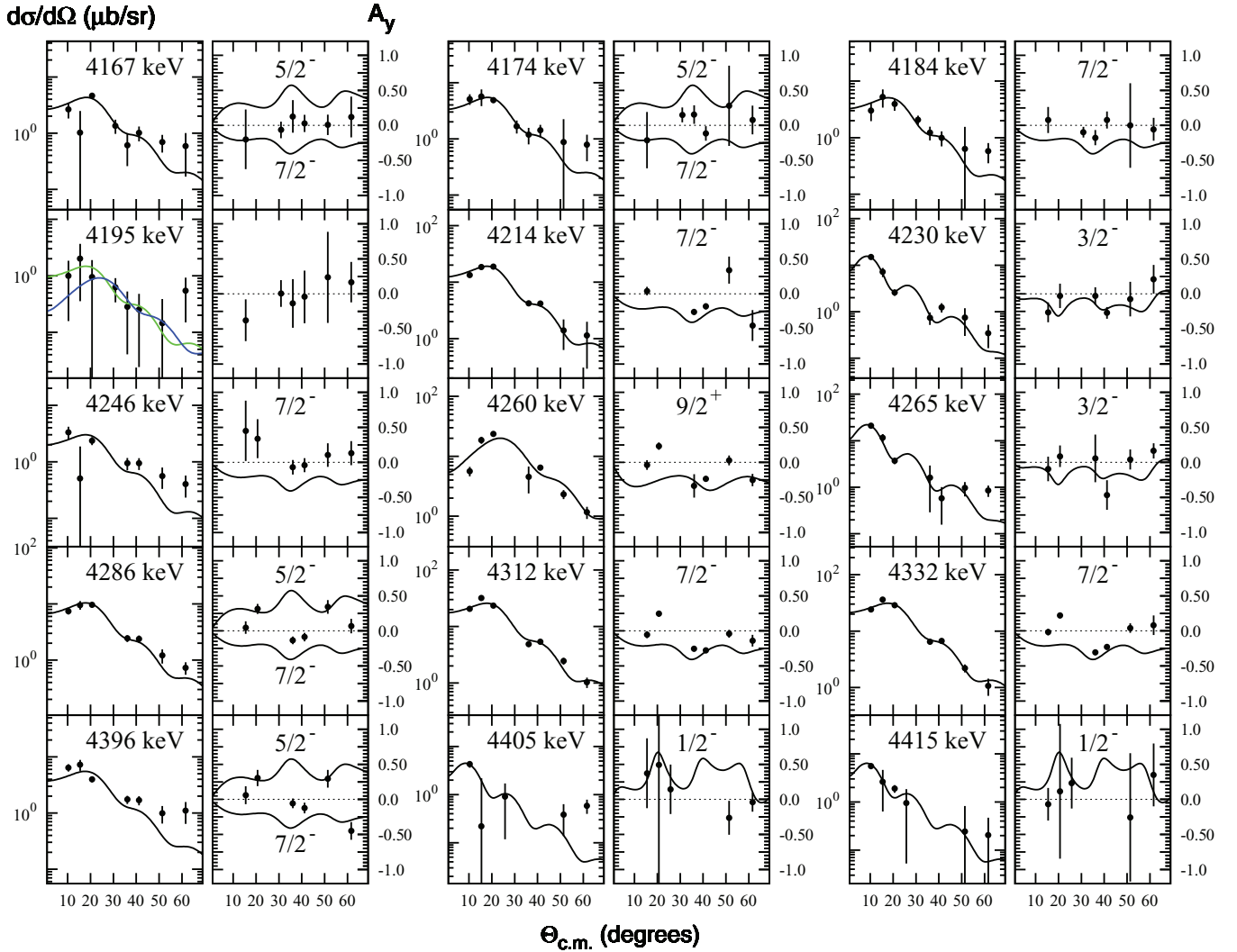
FIG. 12. (Color online) Angular distributions and vector analyzing powers for states populated in ^{63}Zn from 4.2 to 4.4 MeV. For states where multiple L transfers are able to describe the data, both $L = 3$ (green) and $L = 4$ (blue) DWBA calculations are shown.

previous heavy-ion work [39] may in fact be this state, with a slight energy shift. However, in either case, the work presented here cannot provide any additional information due to a lack of low-angle data.

8. 1901- and 1909-keV L = 1 states

This doublet of $L = 1$ states is strongly populated, and they are assigned as $1/2^-$ and $3/2^-$, respectively. There are no states observed previously at these energies; however, if again a slightly shifted energy is adopted relative to that in Ref. [36], these could be the $L = 1$ state at 1924 keV observed in that work, since there was no 1924-keV state observed here.

9. 1978-keV state

This state was previously observed in a (p, γ) reaction from Ref. [38], and the data suggested an assignment of 3/2,

5/2, or 7/2, based on observed γ transitions. Conversely, this state was assigned a $9/2^-$ spin-parity in $(\alpha, n\gamma)$ work [39]. The angular distribution observed in the present work is significantly different from that of the 1435-keV $9/2^-$ level, and is consistent with an $L = 4$ distribution instead. While a fit with the $L = 3$ angular distribution cannot be excluded, the tentative assignment $J^\pi = (9/2^+)$ is made.

10. 2262-keV state

This state was previously observed in the (p, γ) work [38] and assigned as a $5/2^-$ level. The work presented here disagrees with this assignment, and reassigns this state as having $L = 1$, $J^\pi = 1/2^-$.

11. 2378-keV state

The 2378-keV state was populated in this reaction with a small ($\sim$1-μb) cross section, and no L or J assignment
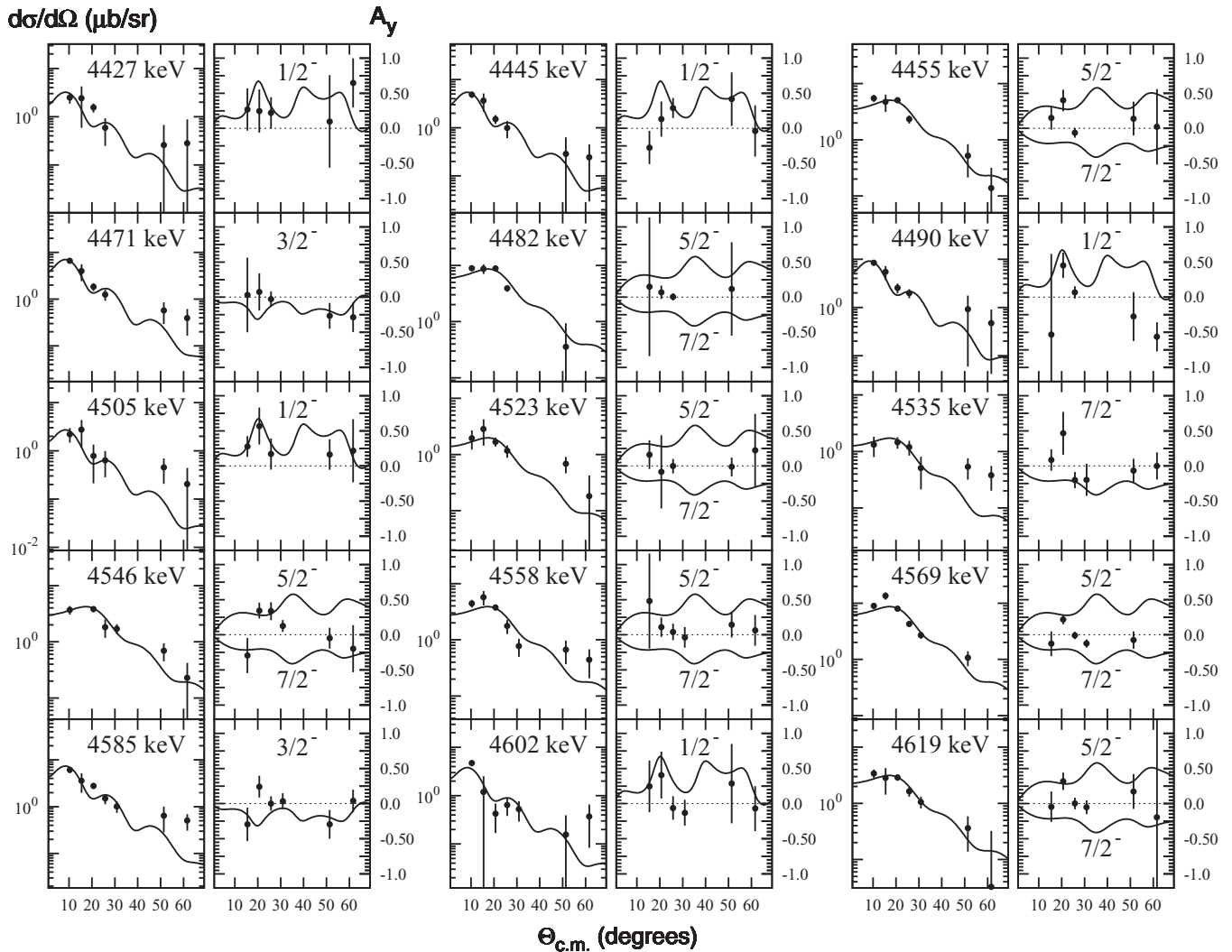
FIG. 13. Angular distributions and vector analyzing powers for states populated in ^{63}Zn from 4.4 to 4.6 MeV.

could be made. This state was previously observed in both (p, γ) and ^{50}Cr(^{16}O, $2pn\gamma$), where an assignment of $9/2^+$ was made. If this state is in fact a $9/2^+$ level, the associated DWBA calculation should be able to reproduce the observed angular distribution in this work, but it does not. No further conclusions can be made regarding this level.

12. 2404-keV state

An assignment of $7/2^-$ for this state is made in this work, with no ambiguity. The previous assignment of this level as $5/2^-$ from the (p, γ) work in Ref. [38] is refuted.

13. 2522-keV state

This level has been previously observed and is assigned a spin-parity of $3/2^-$ from the $(p, n\gamma)$ [38], $(\vec{p}, d)$ [37,41], and $(^3$He, $\alpha)$ [4,36] reactions. Since a clear distinction between $L = 1$ or 3 cannot be made, this work adopts the previous assignment of $3/2^-$, which is shown in brackets in Fig. 6

14. 2610-keV state

This state was also observed in Ref. [38]; however, no spin-parity assignment was made. An $L = 1$ assignment is possible from the data presented in this work; however, no *J* assignment could be made

15. 2910-keV state

This state was populated in this work with cross sections of $\sim$5–10 μb; however, no DWBA calculated curve could describe the angular distribution. This state was also observed in the (p, γ) work in Ref. [38], where a $9/2^{(\pm)}$ assignment was made. In principle, if it were a $9/2^+$ state, it may be be populated in this reaction and described by the DWBA curve. Since this is not the case, it is proposed that this state may be a $9/2^-$ level.

16. Remaining 7/2⁻ states

Many of the remaining levels reported in the previous single-neutron pickup reactions [4,35–39,41] are $7/2^-$ states, which is consistent with the observation of strength seen in
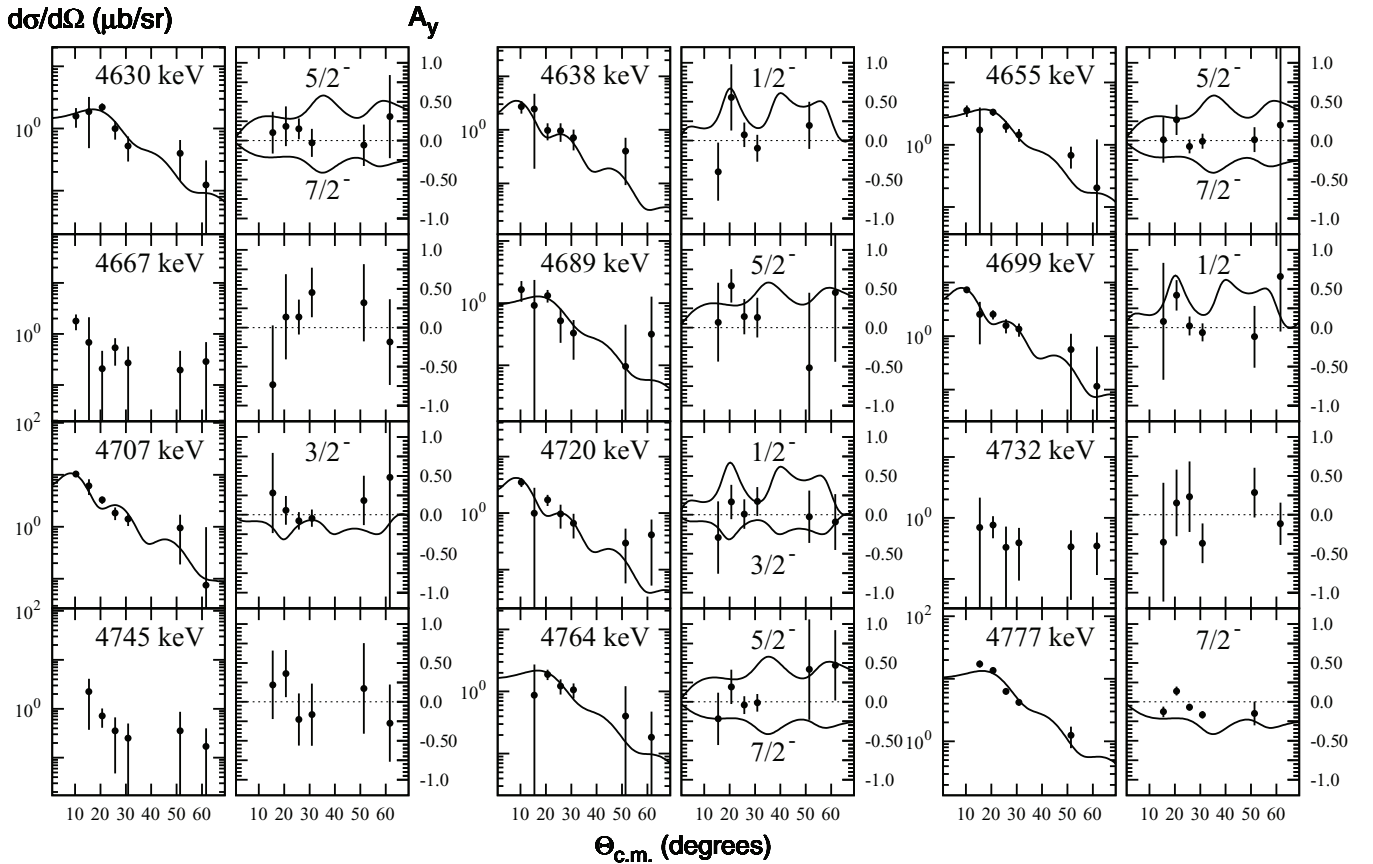
FIG. 14. Angular distributions and vector analyzing powers for states populated in ^{63}Zn from 4.6 to 4.8 MeV.

the work presented here. The previously determined energies of these states are not well known, and it is assumed that they are correlated to the strongly populated $7/2^-$ states observed in this work.

17. $9/2^-$ and $11/2^-$ states

Six possible $9/2^-$ states (1435, 1862, 2051, 2250, 2378, and 2910 keV) and two $11/2^-$ states (2237 and 2318 keV) were observed in this work and identified through a comparison with the evaluated data in Ref. [25]. The population of these levels cannot be described by using a single-particle DWBA description of the ^{64}Zn($\vec{d}, t$)^{63}Zn reaction presented here. Some of these states have angular distributions that are nearly flat, indicating the population of the level through a multi-step process. The assignments of these states are adopted from the evaluation in Ref. [25], which are primarily taken from ($p, n\gamma$), ($\alpha, n\gamma$), and ^{50}Cr(^{16}O, $2pn\gamma$) work. These states are interpreted as $5/2^- \otimes 2^+$ or $7/2^- \otimes 2^+$ states involving the ^{62}Zn core 2^+. By using the evaluated data, an examination of the multi-step contributions which populated these states from this reaction is depicted in Fig. 16, along with their measured $B(E2)$ values for the respective γ transitions.

B. New levels

Due to the high statistics, excellent energy resolution, and comprehensive final-state excitation energy coverage achieved

in this work, the majority of the levels presented are newly observed. Although the evaluated data [25] include many states in ^{63}Zn above 3 MeV, the majority are from heavy-ion reactions which selectively populate high-spin states that are not observed here. For those states which are not described by a pure single-particle transfer, or were very weakly populated, no definite interpretation can be made. All of the observed levels are listed in Table II with their respective level energies and, if possible, their determined spin, parity, and C^2S values. The corresponding angular distributions are shown in Figs. 4–14.

C. Strength distribution

Using the prescription outlined in Sec. III B, experimental C^2S values for ^{63}Zn were extracted up to an energy of $\sim$4.8 MeV, where possible. The strength distribution is displayed as a function of excitation energy in Fig. 15. An examination of the strength distribution shows concentrated $2p_{3/2}$ and $1f_{5/2}$ single-particle characteristics for both the ground state and the 193-keV first-excited state, respectively. The majority of the $2p_{1/2}$ strength is distributed between two states at 248 and 627 keV and accounts for the bulk of the total spectroscopic strength of $\sim$0.3 observed. With a summed strength of $>$1, the $1f_{7/2}$ orbital shows a significant total spectroscopic strength. However, unlike the $2p_{3/2}$ and $1f_{5/2}$ orbitals, this strength is highly fragmented among many levels above
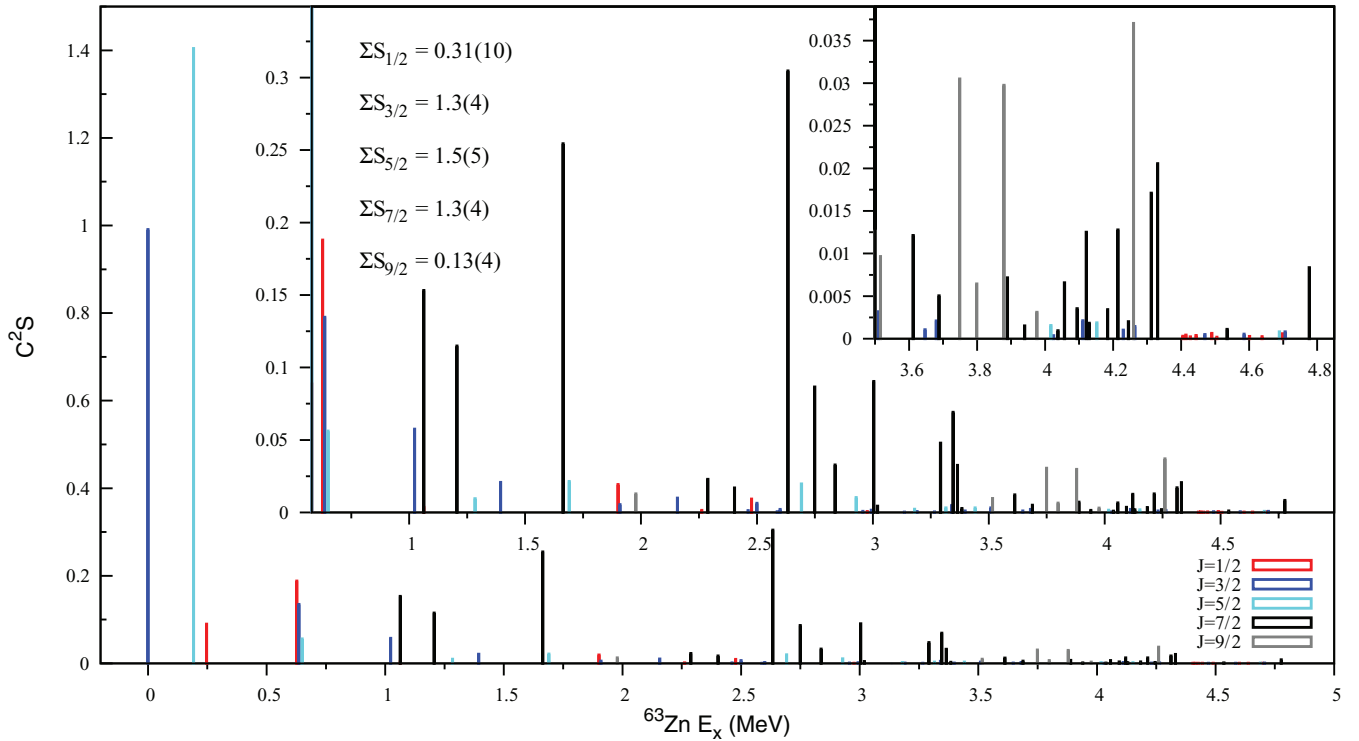
FIG. 15. (Color online) Experimental spectroscopic factors on a level-by-level basis for states populated via $J = 1/2$, $3/2$, $5/2$, $7/2$, and $9/2$ transfers. Due to the concentration of $3/2$ and $5/2$ strength below 200 keV, the remaining region to 5 MeV is expanded in the two insets to show the fragmented strength distribution of weakly populated states. The summed single-particle strength for each orbital is shown in the inset, where the uncertainties quoted include the 30% model-dependent systematic.

1 MeV. Very little $1g_{9/2}$ strength was observed below 4.8 MeV, suggesting that an excitation of particles into this orbital must lie at higher energies. A comparison of these experimentally observed strengths with the shell-model predictions is made in Sec. VI.

V. SHELL-MODEL SPECTROSCOPIC FACTORS

A. MSDI3, MSDI4, and GXPF1

The shell-model calculations of Ref. [5] utilize a closed ^{56}Ni core with three active orbitals ($p_{3/2}$, $f_{5/2}$, and $p_{1/2}$); there are no truncations needed in this model space since the ^{56}Ni core is not open to interaction. The effective shell-model interaction used in these calculations was a modified surface-delta interaction (MSDI) with parameters from Koops and Glaudemans [42].

Conversely, the more recent calculations of Ref. [3] make use of both the MSDI [42] and GXPF1 [43,44] interactions. The result used in the calculation for the ^{62}Ga δ_{C2} value quoted in Ref. [3] used an average of the ^{61}Zn results for each interaction. These calculations use a closed ^{56}Ni core for ^{64}Zn(^{62}Zn) but allow one hole in the $f_{7/2}$ shell for ^{63}Zn(^{61}Zn). Since opening a core-orbital ν hole drastically increases the size of the Hamiltonian matrix in the calculation, further truncations are therefore required. The decision as to how these truncations are performed depends on which orbital

configurations have the strongest wave function contributions to the Hamiltonian. This adds a strongly model-space-dependent uncertainty to the calculations; however, the goal is to retain all of the important configurations in the model space.

The above works [3,5] used calculations explicitly for the system of ^{62}Zn $\rightarrow$ ^{61}Zn; however, in order to directly compare to the ^{64}Zn($\vec{d}, t$)^{63}Zn experiment conducted here, the present work presents the corresponding calculations for the ^{64}Zn $\rightarrow$ ^{63}Zn system. For the case of calculations performed using the MSDI3 interaction, the lowest 50 states for each of $p_{3/2}$, $f_{5/2}$, and $p_{1/2}$ orbitals in ^{64}Zn $\rightarrow$ ^{63}Zn were calculated. No additional truncations are necessary since the calculation is tractable within the model space.

Furthermore, by assuming the same approach as in 2008, spectroscopic factors were calculated for the lowest 100 states for $f_{7/2}$ orbitals and again the lowest 50 for $p_{3/2}$, $f_{5/2}$, and $p_{1/2}$. In this case, in order to make the calculations feasible, further truncations are required within the $f_{7/2}$ states. For the MSDI calculation, the same interaction as that of Ref. [42] was used; however, since the core has been opened for interactions, single-particle energies for ^{40}Ca were adjusted until the correct energies in ^{57}Ni are reproduced. The GXPF1 interaction, however, was intended for untruncated use in the pf shell. Since there is only one hole in the ^{56}Ni core, the single-particle energies were again adjusted to obtain the correct energies in ^{57}Ni.

TABLE II. A complete list of all observed levels in ^{63}Zn, including measured energies, spin-parity assignments, differential cross sections at 30°, and extracted C^2S values. The levels without J^π assignments are levels in ^{63}Zn which were observed but for which no information about the L or J transfer could be extracted. The uncertainties quoted for the C^2S values include the 5% target thickness systematic but do not include the systematic due to model-dependent effects outlined in Sec. III B 1. For states where 30° data are unavailable, 25°(‡) or 20°(△) cross sections are reported. Due to the dramatic drop-off in spectroscopic strengths after the first two states, C^2S values are reported $\times 10^3$ for clarity. States which have been previously observed are denoted with †; all other states shown are new. The known states in ^{63}Zn used in the energy calibration of the Q3D focal plane are denoted with an asterisk next to the energy.

	E_{exp} (keV)	J^π_{exp}	$d\sigma/d\Omega$ (μb/sr)	C^2S ($\times 10^3$)
†	0(0)	$3/2^-$	2274(165)	991(22)
†	192.94(12)*	$5/2^-$	299(22)	1404(33)
†	247.8(2)*	$1/2^-$	199(15)	90(2)
†	627.06(5)*	$1/2^-$	434(31)	188(4)
†	636.83(16)*	$3/2^-$	337(24)	135(3)
†	650.6(5)*	$5/2^-$	13.0(17)	56(2)
†	1023.70(2)*	$3/2^-$	154(11)	57.5(14)
†	1063.73(7)	$1/2^-$	69(5)	3.6(6)
†		$7/2^-$		153(6)
†	1206.54(10)*	$7/2^-$	34(3)	115(3)
†	1284.2(2)*	$5/2^-$	2.1(5)	9.5(6)
†	1394.71(10)*	$3/2^-$	58(4)	20.8(6)
†	1435.37(14)*	–	6.3(9)	
†	1664.93(2)*	$7/2^-$	71(5)	254(9)
	1678.0(2)	$5/2^-,7/2^-$	2.1(8)	
†	1690.67(18)*	$5/2^-$	4.7(5)	21.4(15)
†	1702.66(6)*	$L = 1, 3$	28(2)	
†	1862.5(4)	–	0.5(2)	
	1901.48(11)	$1/2^-$	57(4)	19.3(7)
†	1909.18(10)	$3/2^-$	10.6(13)	5.4(3)
†	1978.24(5)	$(9/2^+)$	3.9(5)	12.8(10)
†	2050.9(7)	–	0.4(2)	
†	2157.74(11)*	$3/2^-$	26(2)	10.0(3)
†	2213.6(2)	–	1.8(3)	
†	2236.8(7)	–	0.3(2)	
†	2250.4(5)	–	1.5(3)	
†	2262.0(3)*	$1/2^-$	4.5(5)	1.52(12)
†	2288.42(5)	$7/2^-$	10.2(9)	22.8(9)
†	2318.37(5)	–	2.3(4)	
	2367.1(5)	–	0.2(3)	
†	2377.67(18)	–	1.8(3)	
†	2403.54(6)*	$7/2^-$	7.1(7)	16.9(8)
	2462.75(9)	$3/2^-$	3.7(4)	1.33(11)
	2477.15(12)	$1/2^-$	31(2)	9.3(3)
	2500.69(14)	$3/2^-$	17.9(14)	6.4(2)
†	2522.16(9)*	$L = 1, 3$	2.0(3)	
	2588.18(16)	$3/2^-$	1.9(4)	0.57(7)
†	2600.58(8)*	$3/2^-$	7.7(8)	2.08(12)
†	2610.1(2)	$1/2^-,3/2^-$	1.9(5)	
†	2634.51(5)*	$7/2^-$	90(7)	305(7)
	2645.1(6)	–	4.6(10)	
	2692.2(6)	$5/2^-$	5.7(6)	19.7(9)

TABLE II. (*Continued.*)

	E_{exp} (keV)	J^π_{exp}	$d\sigma/d\Omega$ (μb/sr)	C^2S ($\times 10^3$)
†	2749.77(10)*	$7/2^-$	26(2)	87(2)
	2769.3(2)	$5/2^-,7/2^-$	0.6(3)	
	2781.3(3)	–	1.0(4)	
†	2837.5(2)	$7/2^-$	9.7(9)	32.8(12)
	2856.0(3)	–	6.0(7)	
	2869.7(5)	$L = 1, 3$	1.1(4)	
	2890.6(5)	$5/2^-,7/2^-,9/2^+$	1.1(3)	
†	2910.3(4)	–	3.5(5)	
	2928.8(5)	$5/2^-$	5.4(7)	10.3(7)
	2957.2(5)	$3/2^-$	2.2(4)	0.74(7)
	2976.9(7)	$1/2^-$	1.8(4)	0.62(7)
	2993.9(5)	$3/2^-$	4.1(6)	1.61(10)
†	3004.0(5)	$7/2^-$	29(2)	90(2)
	3020.3(6)	$7/2^-$	1.5(4)	4.4(6)
	3047.6(8)	–	1.7(4)	
	3061.7(5)	–	3.1(5)	
	3079.8(8)	$5/2^-,7/2^-,9/2^+$	2.1(5)	
	3088.2(6)	–	1.4(4)	
	3108.0(7)	–	0.2(3)	
	3121.1(8)	–	0.5(3)	
	3136.1(6)	$3/2^-$	0.5(3)	0.21(5)
	3164.9(10)	–	4.9(6)	
	3180.1(17)	$5/2^-$	0.8(6)	2.2(5)
	3191(3)	$3/2^-$	1.7(4)	0.70(7)
	3204.5(11)	$L = 1, 3$	2.2(4)	
	3215.3(8)	$5/2^-,7/2^-$	1.7(4)	
	3233.8(15)	$L = 1, 3$	0.4(3)	
	3249.2(11)	$5/2^-,7/2^-$	1.1(10)	
	3266.5(12)	$3/2^-$	1.1(4)	0.39(7)
	3292.5(10)	$7/2^-$	16.8(14)	47.9(15)
	3315.3(13)	$5/2^-$	1.4(4)	3.2(5)
	3340.4(10)	$3/2^-$	15.8(17)	4.9(2)
	3346.3(9)	$7/2^-$	27(2)	69(3)
	3365.5(10)	$7/2^-$	11.7(11)	32.4(11)
	3384.9(14)	$7/2^-$	1.1(3)	2.7(4)
	3398.1(12)	$3/2^-$	3.6(5)	1.00(8)
	3441.8(12)	$5/2^-$	1.1(3)	3.1(4)
	3509.4(11)	$3/2^-$	9.8(11)	3.16(16)
	3516.5(10)	$9/2^+$	2.5(7)	9.7(13)
	3559(3)	–	0.5(3)	
	3580.8(14)	–	0.8(3)	
	3612.0(12)	$7/2^-$	5.5(6)	12.1(6)
	3634.9(11)	$5/2^-,7/2^-$	1.5(4)	
	3647.7(11)	$3/2^-$	2.7(5)	1.05(8)
	3668.1(7)	–	0.3(3)	
	3680.2(10)	$3/2^-$	6.0(8)	2.09(13)
	3688.5(5)	$7/2^-$	2.0(6)	5.0(6)
	3723.7(15)	–	0.6(3)	
	3735.7(11)	–	2.0(3)	
	3749.5(9)	$9/2^+$	12.6(11)	30.5(14)
	3756.5(10)	$5/2^-,7/2^-$	1.7(6)	
	3767.5(13)	–	1.3(5)	
	3781.7(11)	–	0.8(3)	
	3799.1(8)	$9/2^+$	2.6(3)	6.4(4)
	3829(9)	–	0.7(4)	
	3836(4)	$5/2^-,7/2^-$	1.0(4)	
	3844(4)	–	0.4(5)	

TABLE II. (*Continued.*)

$E_{\exp}$ (keV)	$J^\pi_{\exp}$	$d\sigma/d\Omega$ (μb/sr)	C^2S ($\times 10^3$)
3862(2)	–	0.3(2)	
3879.8(5)	$9/2^+$	11.1(10)	29.8(11)
3889.2(6)	$7/2^-$	3.4(5)	7.1(4)
3899.6(10)	$5/2^-,7/2^-$	0.8(3)	
3916.5(15)	–	1.2(4)	
3923.9(8)	–	6.3(7)	
3932.4(19)	–	1.4(3)	
3940.5(15)	$7/2^-$	0.3(3)	1.5(2)
3976.8(9)	$9/2^+$	1.4(3)	3.1(4)
3997(2)	–	1.0(3)	
4004(2)	–	0.6(3)	
4017.9(13)	$5/2^-$	0.9(3)	1.5(3)
4026.0(13)	$3/2^-$	0.8(3)	0.36(5)
4039(4)	$7/2^-$	0.4(2)	0.9(2)
4057.6(13)	$7/2^-$	2.8(4)	6.6(5)
4067(5)	–	0.4(7)	
4079.6(15)	–	0.7(6)	
4094.5(14)	$7/2^-$	2.1(3)	3.5(3)
4111.6(12)	$3/2^-$	4.4(5)	2.10(10)
4121.4(13)	$7/2^-$	5.5(6)	12.5(7)
4130(2)	$7/2^-$	0.5(3)	1.8(4)
4152.8(15)	$5/2^-$	0.9(3)	1.9(2)
4167(2)	$5/2^-,7/2^-$	1.4(4)	
4174.2(18)	$5/2^-,7/2^-$	1.7(4)	
4184.1(19)	$7/2^-$	2.1(4)	3.4(4)
4195(4)	$5/2^-,7/2^-,9/2^+$	0.6(3)	
4214.1(16)	$7/2^-$	18.8(11)$^\triangle$	12.8(5)
4230.1(19)	$3/2^-$	2.6(4)$^\triangle$	1.01(7)
4245.5(19)	$7/2^-$	2.3(4)$^\triangle$	2.0(2)
4260(2)	$9/2^+$	23.5(14)$^\triangle$	37.0(17)
4265(3)	$3/2^-$	3.7(6)$^\triangle$	1.44(9)
4286.5(19)	$5/2^-,7/2^-$	9.7(7)$^\triangle$	
4312.1(19)	$7/2^-$	23.5(14)$^\triangle$	17.1(6)
4332(2)	$7/2^-$	28.8(16)$^\triangle$	20.6(7)
4396(2)	$5/2^-,7/2^-$	4.0(5)$^\triangle$	
4405(3)	$1/2^-$	0.9(8)‡	0.30(5)
4415(3)	$1/2^-$	0.9(9)‡	0.43(5)
4427(2)	$1/2^-$	0.6(3)‡	0.22(4)
4445(2)	$1/2^-$	1.0(4)‡	0.37(4)
4455(3)	$5/2^-,7/2^-$	2.3(4)‡	
4471(3)	$3/2^-$	1.3(3)‡	0.49(5)
4482(3)	$5/2^-,7/2^-$	3.9(5)‡	
4490(3)	$1/2^-$	2.0(4)‡	0.63(5)
4505(3)	$1/2^-$	0.6(4)‡	0.19(5)
4523(3)	$5/2^-,7/2^-$	1.2(3)‡	
4535(3)	$7/2^-$	0.5(3)	1.10(17)
4546(3)	$5/2^-,7/2^-$	1.7(4)	
4558(3)	$5/2^-,7/2^-$	0.8(3)	
4569(3)	$5/2^-,7/2^-$	2.7(4)	
4585(3)	$3/2^-$	1.0(3)	0.53(5)
4602(3)	$1/2^-$	0.5(2)	0.27(4)
4619(3)	$5/2^-,7/2^-$	1.1(3)	
4630(4)	$5/2^-,7/2^-$	0.5(2)	
4638(3)	$1/2^-$	0.7(3)	0.25(4)
4655(4)	$5/2^-,7/2^-$	1.4(3)	
4667(4)	–	0.3(3)	
4689(3)	$5/2^-$	0.3(2)	0.81(15)

TABLE II. (*Continued.*)

$E_{\exp}$ (keV)	$J^\pi_{\exp}$	$d\sigma/d\Omega$ (μb/sr)	C^2S ($\times 10^3$)
4699(4)	$1/2^-$	1.3(4)	0.59(5)
4707(4)	$3/2^-$	1.4(4)	0.80(6)
4720(4)	$1/2^-,3/2^-$	0.7(3)	
4732(5)	–	0.4(3)	
4745(4)	–	0.2(2)	
4764(4)	$5/2^-,7/2^-$	1.1(3)	
4777(4)	$7/2^-$	4.2(5)	8.4(4)

The currently adopted ISB correction calculations of Towner and Hardy [1,3] use the MSDI4 and GXPF1 interactions to compute δ_{C2} for the $^{62\to61}$Zn system. The relative contributions to δ_{C2} for the different orbitals are given in Table IV, and they demonstrate the effect of the radial-mismatch factor weighting on the final correction value, as calculated using Eq. (5). For the high-ℓ orbitals, the radial-mismatch factor is relatively small, implying that the accuracy in the calculation of S for these states is less important than that for the $j = 1/2$ and $3/2$ orbitals, since these orbitals are $2p$ orbitals with a radial node. The presence of a radial node gives a greater sensitivity to the ISB in the radial overlap integral. As a result, the radial-mismatch factors $\Omega_{1/2}$ and $\Omega_{3/2}$ are nearly three times larger than those for $j = 5/2$ and $7/2$, and since the calculated $\sum_\pi S^\pi_\alpha$ for the $3/2$ orbital is much larger than that for the $1/2$ orbital, it carries the largest weight in the overall δ_{C2} sum.

B. GXPF1A

As a comparison to the current superallowed ISB theory shell-model employed by Towner and Hardy [3], the ^{64}Zn $\to$ ^{63}Zn spectroscopic factors were also calculated using the GXPF1A interaction [45], and are presented here.

These calculations were performed in the pf shell with up to two proton holes and up to two neutron holes in the $1f_{7/2}$ orbital relative to the ^{56}Ni closed core. The J-scheme

TABLE III. A comparison of the number of observed levels for each orbital to the theoretically predictions from each of the three respective shell-model interactions. The experimental values are lower limits, since definite J^π values for all observed states could not be determined. In order to provide an accurate comparison of what would be observed, only states with a predicted $C^2S \geqslant 0.0001$ are included in the sums.

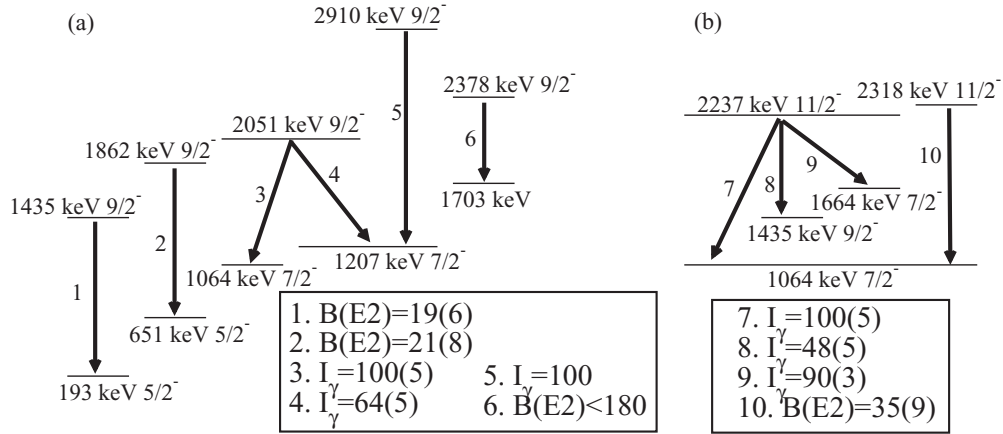| Orbital	Expt. lower limit	MSDI3	MSDI4	GXPF1	GXPF1A
$2p_{1/2}$	16	31	26	12	22
$2p_{3/2}$	27	41	45	21	44
$1f_{5/2}$	12	46	46	18	42
$1f_{7/2}$	29	–	48	23	47
$1g_{9/2}$	7	–	–	–	–
Total	91	118	165	74	165

FIG. 16. The multistep population process for (a) $9/2^-$ and (b) $11/2^-$ states observed in this experiment. The arrows show the observed γ-decay paths that are listed in the evaluated data from Ref. [25]. Where known, $B(E2)$ values are given for the respective transitions in Weisskopf units (W.u.); otherwise relative γ-ray intensities, I_γ, are listed. These values, for all ten decay paths, are taken from the evaluated data [25].

dimension for ^{64}Zn 0^+ was 421 655 and the J-scheme dimension for ^{63}Zn $7/2^-$ was 3 623 537. By using this increased model space, the lowest 50 states for the $f_{7/2}$, $p_{3/2}$, $f_{5/2}$, and $p_{1/2}$ orbitals were calculated, and these are presented in Sec. VI.

VI. COMPARISON OF DATA WITH THEORETICAL MODELS

A comparison of the present data to the theoretical models shown in Fig. 17 suggests that the relative spectroscopic strengths seem to be reproduced with reasonable accuracy. However, in nearly all cases, the theoretical shell-model predictions overestimate the absolute spectroscopic strengths. Specifically, the $J = 3/2$ orbital, with the largest effect on the overall δ_{C2} sum, is overestimated by all of the shell-model predictions. Of course, the summed strengths reported represent lower limits for each orbital, since they only include states where an identification of the J transfer is possible. In order to quantify an upper limit for states where the L and/or J values were not determined, a running sum of the possible unaccounted strengths were: $2p_{1/2} = 0.036(10)$, $2p_{3/2} = 0.035(10)$, $1f_{5/2} = 1f_{7/2} = 0.28(8)$, and $1g_{9/2} = 0.23(7)$.

With the inclusion of the $1f_{7/2}$ core orbitals into the calculation model space, the most interesting comparison to be made is that of the $J = 7/2$ strength, which is displayed in the

TABLE IV. Illustration of the strategy used in calculating δ_{C2} for ^{62}Ga. The yrast states of each spin and isospin are identified and shown on the left. The average radial-mismatch factor $\overline{\Omega_\alpha^\pi}$ is also given for both interactions, where the averaging is over all parent states, π, of given spin and isospin. Both shell-model calculations show the calculated sum of spectroscopic factors and the contribution to δ_{C2} from all states of that spin and isospin. The consequence of leaving out the $f_{7/2}$ orbital in the calculation is shown in the last line.

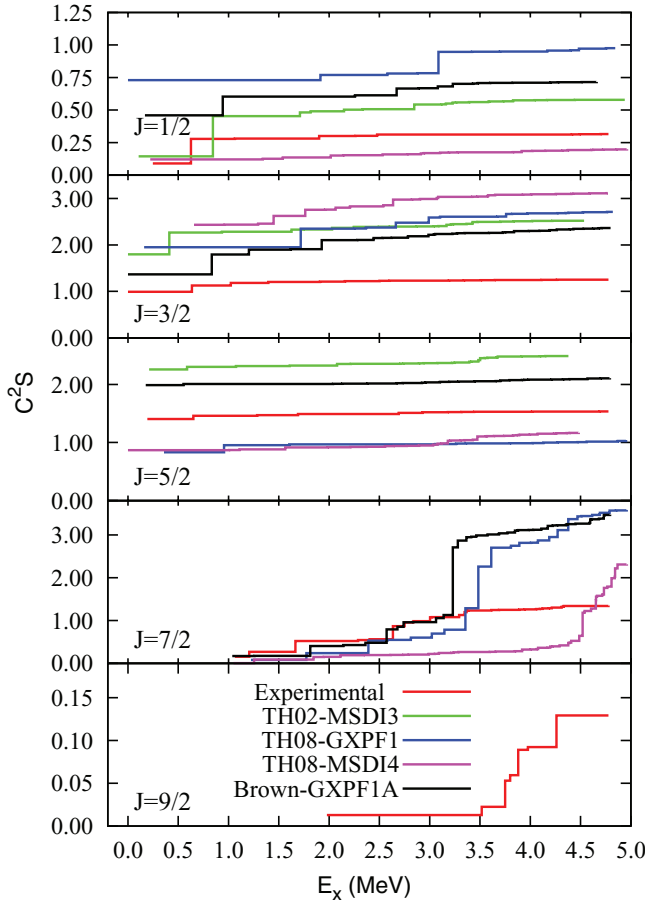| ^{61}Zn E_x (keV)	Yrast $J^\pi; T_\pi$	α	MSDI Shell model $\overline{\Omega_\alpha^\pi}(\%)$	$\sum_\pi S_\alpha^\pi$	Contribution to δ_{C2} (%)	GXPF1 Shell model $\overline{\Omega_\alpha^\pi}(\%)$	$\sum_\pi S_\alpha^\pi$	Contribution to δ_{C2} (%)
0	$\frac{3}{2}^-; \frac{1}{2}$	$p_{3/2}$	0.586	2.13	1.25	0.605	1.94	1.17
88	$\frac{1}{2}^-; \frac{1}{2}$	$p_{1/2}$	0.469	0.21	0.10	0.549	0.57	0.31
124	$\frac{5}{2}^-; \frac{1}{2}$	$f_{5/2}$	0.183	0.94	0.17	0.219	0.64	0.14
996	$\frac{7}{2}^-; \frac{1}{2}$	$f_{7/2}$	0.142	5.33	0.76	0.160	4.52	0.73
3220	$\frac{3}{2}^-; \frac{3}{2}$	$p_{3/2}$	0.393	2.17	−0.43	0.403	1.97	−0.40
3695	$\frac{1}{2}^-; \frac{3}{2}$	$p_{1/2}$	0.316	0.14	−0.02	0.379	0.39	−0.07
4190	$\frac{5}{2}^-; \frac{3}{2}$	$f_{5/2}$	0.121	0.34	−0.02	0.133	0.11	−0.01
4531	$\frac{7}{2}^-; \frac{3}{2}$	$f_{7/2}$	0.117	10.66	−0.62	0.129	9.06	−0.58
Sum					1.19			1.29
Sum excluding $f_{7/2}$					1.06			1.15

FIG. 17. (Color online) A running-sum comparison of the spectroscopic strengths measured here to the shell-model calculations described in Sec. V. Each panel shows the accumulated spectroscopic strength as a function of ^{63}Zn excitation energy for the five respective orbitals. The $1f_{7/2}$ orbital was not included in the TH02-MSDI3 shell-model calculation, and thus it is not present in the above panel. None of the shell-model calculations include the possibility for excitation of particles from the $1g_{9/2}$ orbital; therefore only the experimental data are shown. It should also be noted that the experimental curves represent a lower limit prediction, since only levels where definite J values could be determined are included.

fourth panel of Fig. 17. The three interactions produce slightly different trends in the cumulative sum of the spectroscopic strengths, with the majority of the strength for GXPF1 and GXPF1A produced between 3.5 and 4 MeV, while the MSDI4 sees this increase above 4.5 MeV. Both interactions, however, seem to properly reproduce the general trend up to ~3.5 MeV, but the sudden increase of strength is not observed, at least to the degree at which the two models predict. The GXPF1A calculations suggest that all of this strength is located in one state at 3.23 MeV, while the smaller model space employed in the GXPF1 calculation predicts a similar total strength that is fragmented over three states.

An evaluation of the number of states predicted for each orbital, within each shell-model interaction, was also performed, and the comparison is made in Table III. In this comparison, the total number of experimentally observed levels presented in this work where definite J^π values were able to be determined

are listed for each orbital. Since there were several states where this was not possible, these values represent a lower limit of the potential states that could be observed in this reaction, up to an excitation energy in ^{63}Zn of 4.8 MeV. In addition, to provide a proper comparison of theory to states which could possibly be observed, only those predicted to have a $C^2S \geqslant 1 \times 10^{-4}$ are included.

For the two MSDI shell-model calculations, the number of states observed is generally consistent with the predicted totals, where, in all cases, there are more states predicted than observed. For the GXPF1 interaction, all but the $1f_{5/2}$ orbital predict fewer states than what is observed, which may indicate a need to reevaluate the calculations.

The values listed in Table IV underscore the fact that, to have a significant contribution to δ_{C2}, both S and Ω must be relatively large. As the number of nodes in the radial wave function increases, Ω will naturally become larger; thus the low-ℓ orbitals have more significant Ω values. For S to be large, the orbital must be filled significantly, which occurs for those orbitals below the Fermi surface. Thus, the lack of large $g_{9/2}$ strength observed in the present work suggests that the absence of the $g_{9/2}$ orbital in the model space may, in itself, not be serious. However, it could lead to the absence of deformation effects that result in a major rearrangement of levels in the ^{62}Zn daughter, the position of which can influence the amount of isospin mixing.

It is noted from Fig. 17 that the cumulative strength of the $p_{3/2}$ orbital for the ^{64}Zn($\vec{d}, t$)^{63}Zn reaction is smaller then in all calculations, and the corresponding strength for the $p_{1/2}$ orbital is smaller for all but the MSDI4 interaction. As these orbitals also have the largest Ω values, they contribute significantly to δ_{C2}. While the experimental results for the ^{64}Zn($\vec{d}, t$)^{63}Zn reaction cannot be directly used for the ^{61}Zn calculations, it suggests an overprediction of the spectroscopic strength for the ^{62}Zn($\vec{d}, t$)^{61}Zn reaction as well. This would result in a lowering of both the positive and negative contributions to δ_{C2}, the net result of which could cause a decrease of δ_{C2}, no change, or even an increase in δ_{C2}, depending on the strength distribution into the $T_\pi = 1/2$ and $T_\pi = 3/2$ states.

VII. CONCLUSION

A study of the ^{64}Zn($\vec{d}, t$)^{63}Zn reaction was conducted with 22-MeV incident deuterons, and the reaction products were mass-analyzed using a Q3D magnetic-spectrograph, with a final-state energy resolution of ~8 keV. Angular distributions and vector analyzing powers were constructed for states in ^{63}Zn, up to an excitation energy of 4.8 MeV. A study of the suitability for several global optical-model parameter sets was conducted for both deuterons and tritons by comparing the DWBA prediction to the respective elastic scattering data. The optimal OMP sets were used in the DWBA calculations presented in this work to extract experimental spectroscopic factors for all states where I^π assignments could be made. An evaluation of the optical model dependencies was also conducted, and it was determined that the spectroscopic factors extracted using all possible combination of deuteron and triton OMP sets were within 30% of one another.

Both the $2p_{3/2}$ and $1f_{5/2}$ orbitals show highly single-particle characteristics, with the majority of their strength located in the ground state and first-excited states, respectively. The total $1f_{7/2}$ strength is significant; however, it is highly fragmented among states above 1 MeV.

Shell-model calculations for the ^{64}Zn $\rightarrow$ ^{63}Zn system have also been performed, using the same prescription as Refs. [3,5] for ^{62}Zn $\rightarrow$ ^{61}Zn, which is relevant for ISB corrections in the ^{62}Ga superallowed β-decay system. A comparison of the extracted C^2S values to the predicted shell-model spectroscopic factors was conducted, revealing an overall over-prediction of strength for the $2p_{3/2}$ orbital, as well as a large disagreement for the $1f_{7/2}$ orbital above $\sim$3.5 MeV for the GXPF1, GXPF1A, and MSDI4 interactions. Due to the large effect of the $2p_{3/2}$ orbital on the δ_{C2} sum for the $^{62\rightarrow61}$Zn system (Table IV), the overprediction of strength for this orbital in $^{64\rightarrow63}$Zn may have a significant effect on the ^{62}Ga δ_C correction. It should be noted, however, that recent work [46] has shown that there is a systematic quenching of spectroscopic strengths in single-neutron knockout reactions for $N \approx Z$ nuclei of $\sim$0.6. If this systematic reduction is considered, the MSDI3 and GXPF1A results in Fig. 17 for $J = 1/2$, 3/2, and 5/2 are closer to the experimental results, and the effect of the overprediction of strength for the $2p_{3/2}$ orbital may be lessened. However, even a discrepancy of 25% may have a large effect on δ_{C2}, due to its large radial-mismatch factor.

No significant $1g_{9/2}$ strength was observed, suggesting that this orbital does not play a role in excitations below 5 MeV,

and thus it does not need to be included in the ISB calculation model space for ^{62}Zn.

In conclusion, the inclusion of $1f_{7/2}$ core orbitals in the ISB calculation model space in Ref. [3] is validated in this work through the observation of significant 7/2 spectroscopic strength. The interactions used in the calculations, however, need to be reexamined to reproduce the observed distribution and magnitude of strength above $\sim$3.8 MeV. Due to its large relative contribution to δ_C, the $2p_{3/2}$ orbital represents the most important part of the sum. If the measured spectroscopic factors for this orbital are similar to ^{61}Zn, it may result in a difference of the extracted δ_{C2} value for ^{62}Ga of up to 50% in this mass region. However, with new theoretical techniques, and large-scale shell-model calculations, future improvements on the ISB calculations for $A \geqslant 64$ will be possible, and may lead to increased precision on the extracted $\mathcal{F}t$ values.

[1] J. C. Hardy and I. S. Towner, Phys. Rev. C **79**, 055502 (2009).

[2] I. S. Towner and J. C. Hardy, Rep. Prog. Phys. **73**, 046301 (2010).

[3] I. S. Towner and J. C. Hardy, Phys. Rev. C **77**, 025501 (2008).

[4] D. D. Borland, Ph.D. thesis, Washington University, 1967.

[5] I. S. Towner and J. C. Hardy, Phys. Rev. C **66**, 035501 (2002).

[6] G. A. Miller and A. Schwenk, Phys. Rev. C **78**, 035501 (2008); **80**, 064319 (2009).

[7] A. Çalik, M. Gerçeklioğlu, and D. I. Salamov, Z. Naturforsch. **64a**, 865 (2009).

[8] W. Satuła, J. Dobaczewski, W. Nazarewicz, and M. Rafalski, Phys. Rev. Lett. **103**, 012502 (2009); **106**, 132502 (2011).

[9] H. Liang, N. V. Giai, and J. Meng, Phys. Rev. C **79**, 064316 (2009).

[10] N. Auerbach, Phys. Rev. C **79**, 035502 (2009).

[11] V. Rodin, arXiv:1206.0491 [nucl-th].

[12] G. F. Grinyer, C. E. Svensson, and B. A. Brown, Nucl. Instrum. Methods A **622**, 236 (2010).

[13] I. S. Towner and J. C. Hardy, Phys. Rev. C **82**, 065501 (2010).

[14] D. H. Wilkinson, Nucl. Instrum. Methods Phys. Res. A **335**, 182 (1993).

[15] M. Bhattacharya et al., Phys. Rev. C **77**, 065503 (2008).

[16] D. Melconian et al., Phys. Rev. Lett. **107**, 182301 (2011); Phys. Rev. C **85**, 025501 (2012).

[17] E. Hagberg, V. T. Koslowsky, J. C. Hardy, I. S. Towner, J. G. Hykawy, G. Savard, and T. Shinozuka, Phys. Rev. Lett. **73**, 396 (1994).

[18] B. K. Jennings, arXiv:1102.3721v1 [nucl-th].

[19] J. P. Schiffer et al., Phys. Rev. Lett. **108**, 022501 (2012).

[20] P. Finlay et al., Phys. Rev. Lett. **106**, 032501 (2011).

[21] B. Hyland et al., Phys. Rev. Lett. **97**, 102501 (2006).

[22] P. Finlay et al., Phys. Rev. C **78**, 025502 (2008).

[23] R. Hertenberger et al., Nucl. Instrum. Methods A **536**, 266 (2005).

[24] H.-F. Wirth, H. Angerer, T. von Egidy, Y. Eisermann, G. Graw, and R. Hertenberger, Maier-Leibnitz-Laboratorium Jahresbericht (2000), p. 71.

[25] Evaluated Nuclear Structure Data, http://www.nndc.bnl.gov/ensdf (database version of January 13, 2012).

[26] P. D. Kunz, computer code DWUCK4, University of Colorado (unpublished).

[27] C. M. Perey and F. G. Perey, At. Data Nucl. Data Tables **17**, 1 (1976).

[28] J. Bojowald, H. Machner, H. Nann, W. Oelert, M. Rogge, and P. Turek, Phys. Rev. C **38**, 1153 (1988).

[29] Y. Han, Y. Shi, and Q. Shen, Phys. Rev. C **74**, 044615 (2006).

[30] H. An and C. Cai, Phys. Rev. C **73**, 054605 (2006).

[31] Experimental Nuclear Reaction (EXFOR) Database, Software Version date 2011.09.23, http://www-nds.iaea.org/exfor/exfor.htm (2011).

[32] K. C. McLean, S. M. Dalgliesh, S. S. Ipson, and G. Brown, Nucl. Phys. A **191**, 417 (1972).

[33] X. Li, C. Liang, and C. Cai, Nucl. Phys. A **789**, 103 (2007).

[34] D. Y. Pang, P. Roussel-Chomaz, H. Savajols, R. L. Varner, and R. Wolski, Phys. Rev. C **79**, 024615 (2009).

[35] M. E. Brandan and W. Haeberli, Nucl. Phys. A **287**, 205 (1977).

[36] M. G. Betigeri, H. H. Duhm, R. Santo, R. Stock, and R. Bock, Nucl. Phys. A **100**, 416 (1967).

[37] P. A. S. Metford, T. Taylor, and J. A. Cameron, Nucl. Phys. A **308**, 210 (1978).

[38] C. T. Papadopoulos, A. C. Xenoulis, P. Bakogiorgos, G. Andritsopoulos, P. A. Assimakopoulos, N. H. Gangas, and A. G. Hartas, Phys. Rev. C **25**, 155 (1982).

[39] O. M. Mustaffa, L. P. Ekstrom, G. D. Jones, F. Kearns, T. P. Morrison, H. G. Price, D. N. Simister, P. J. Twin, R. Wadsworth, and N. J. Ward, J. Phys. G **5**, 1283 (1979).

[40] A. K. Singh *et al.*, Phys. Rev. C **57**, 1617 (1998).

[41] R. R. Johnson and G. D. Jones, Nucl. Phys. A **122**, 657 (1968).

[42] J. E. Koops and P. W. M. Glaudemans, Z. Phys. A **280**, 181 (1977).

[43] M. Honma, T. Otsuka, B. A. Brown, and T. Mizusaki, Phys. Rev. C **65**, 061301(R) (2002).

[44] M. Honma, T. Otsuka, B. A. Brown, and T. Mizusaki, Phys. Rev. C **69**, 034335 (2004).

[45] M. Honma, T. Otsuka, B. A. Brown, and T. Mizusaki, Eur. Phys. J. A **25**, 499 (2005).

[46] A. Gade *et al.*, Phys. Rev. C **77**, 044306 (2008).